A Low-Power Agile Coherent IR-UWB Receiver with Non-Coherent-Assisted Synchronization

by

Amin POURVALI KAKHKI

MANUSCRIPT-BASED THESIS PRESENTED TO ÉCOLE DE TECHNOLOGIE SUPÉRIEURE
IN PARTIAL FULFILLMENT OF A MASTER'S DEGREE
WITH THESIS IN ELECTRICAL ENGINEERING
M.A.Sc.

MONTREAL, DECEMBER 22, 2022

ÉCOLE DE TECHNOLOGIE SUPÉRIEURE
UNIVERSITÉ DU QUÉBEC

BOARD OF EXAMINERS

THIS THESIS HAS BEEN EVALUATED

BY THE FOLLOWING BOARD OF EXAMINERS

Mr. Frederic Nabki, Thesis supervisor
Department of Electrical Engineering, École de technologie supérieure

Mr. Dominic Deslandes, Chair, Board of Examiners
Department of Electrical Engineering, École de technologie supérieure

Mr. Claude Thibeault, Member of the Jury
Department of Electrical Engineering, École de technologie supérieure

THIS THESIS WAS PRESENTED AND DEFENDED

IN THE PRESENCE OF A BOARD OF EXAMINERS AND THE PUBLIC

ON NOVEMBER 29, 2022

AT ÉCOLE DE TECHNOLOGIE SUPÉRIEURE

FOREWORD

I would like to express my gratitude and appreciation to my supervisor Professor Frederic Nabki whose unconditional guidance, unlimited support, and encouragement have been invaluable throughout this study and have greatly contributed to the outcome.

I also wish to thank Professor Mohammad Taherzadeh-sani at the Department of Electrical Engineering, Ferdowsi University of Mashhad, Iran, for all his guidance, and outstanding feedback.

Un récepteur IR-UWB cohérent agile à faible puissance avec synchronisation non cohérente assistée

Amin POURVALI KAKHKI

RÉSUMÉ

Impulse Radio Ultra Wide Band (IR-UWB) a récemment reçu une attention particulière pour les applications de communication sans fil à courte portée. Les propriétés uniques des systèmes IR-UWB les ont rendus plus répandus dans les résaux de capteurs sans fil et Internet of Things (IoT), les appareils intelligents et les téléphones intelligents d'aujourd'hui.

Une variété d'architectures d'émetteurs-récepteurs IR-UWB ont été proposées par les chercheurs au cours de la dernière décennie, y compris des architectures cohérentes et non cohérentes qui peuvent améliorer une ou plusieurs propriétés associées aux systèmes IR-UWB. Ce mémoire vise à réaliser un système IR-UWB cohérent à faible consommation d'énergie. Afin de réduire la consommation énergétique des récepteurs cohérents classiques, un algorithme hybride de synchronisation des récepteurs cohérents est proposé. Préalablement à une synchronisation cohérente, l'algorithme utilise une synchronisation assistée non cohérente pour limiter l'espace de recherche. Par rapport aux récepteurs cohérents conventionnels, ce procédé réduit considérablement la quantité d'énergie utilisée pour la synchronisation.

La méthode de synchronisation hybride proposée commence par un mécanisme de synchronisation non cohérent basé sur la détection d'énergie utilisant la modulation On-Off Keying (OOK) pour synchroniser grossièrement le récepteur en déterminant la bonne fenêtre d'intégration dans laquelle réside le signal reçu. Une fois que le niveau de synchronisation est atteint de façon grossière, une corrélation cohérente basée sur un modèle cohérent employant une modulation Binary Phase-Shift Keying (BPSK) est effectuée pour une synchronisation fine.

Un prototype de récepteur IR-UWB fonctionnant de 3,5 à 5 GHz a été implémenté dans une technologie TSMC CMOS 65 nm. Notre architecture de récepteur proposée nous a permis de comparer notre approche de synchronisation hybride à deux architectures de récepteur courantes, à savoir les récepteurs de détection d'énergie non cohérents et ceux cohérents.

L'architecture du récepteur utilise un auto-mélangeur pour une détection non cohérente basée sur la modulation OOK et une corrélation de modèle pour une détection cohérente basée sur la modulation BPSK. La plupart des blocs de l'architecture du récepteur proposée, y compris le LNA, le mélangeur et les circuits de bande de base, sont partagés entre les modes non cohérents et cohérents afin de minimiser la consommation d'énergie totale et la zone de réception. Un mécanisme d'acquisition grossière et fine en deux étapes est utilisé pour simplifier la synchronisation cohérente et minimiser la longueur de paquet totale requise. Un Delay-Locked Loop (DLL) avec multi-résolution et un Voltage Controlled Oscillator (VCO) avec démarrage rapide fournissent la phase appropriée pour la fenêtre d'intégration et la génération de modèles.Une DLL multi-résolution et un VCO à démarrage rapide fournissent la phase adéquate pour l'intégration et la génération d'impulsions modèles.

Le récepteur consomme 6,8 mW en mode non cohérent et 8,8 mW en mode cohérent lorsqu'il est toujours activé, à l'exclusion de la consommation d'énergie des circuits tampons et du processeur de bande de base numérique. Il atteint une sensibilité RF de -68 dBm, -70,5 dBm et -70,8 dBm à un Bit Error Rate (BER) de 10^{-3} en mode non cohérent, cohérent et en mode hybride proposé, respectivement. Notre architecture de récepteur proposée, en combinaison avec l'algorithme de synchronisation hybride, démontre que l'approche de synchronisation proposée est capable de réduire considérablement le temps requis pour le préambule. La durée des paquets est réduite de 37,12 μs dans le cas de corrélation cohérente à 24,42 μs avec la méthode de synchronisation hybride proposée pour une charge utile de 1024 bits.

Mots-clés: Ultra-wideband, impulse radio, coherent, non-coherent, synchronization, low power, template-based correlation

A Low-Power Agile Coherent IR-UWB Receiver with Non-Coherent-Assisted Synchronization

Amin POURVALI KAKHKI

ABSTRACT

Impulse Radio Ultra Wide Band (IR-UWB) has recently received significant attention for short-range wireless communication applications. The unique properties of IR-UWB systems have made them more prevalent in today's wearable and Internet of Things (IoT), sensor nodes, healthcare devices and smartphones.

A variety of transceiver architectures in the IR-UWB system have been proposed by researchers over the past decade, including coherent and non-coherent architectures, which can improve one or more challenges associated with the IR-UWB systems. This thesis aims to realize a low-power efficient coherent IR-UWB system. In order to reduce the energy consumption of conventional coherent receivers, a hybrid synchronization algorithm for the coherent receivers is proposed. Prior to a coherent synchronization, the algorithm uses a non-coherent assisted synchronization to limit the search space. Compared to conventional coherent receivers, this method greatly reduces the amount of power used for receiver synchronization.

The proposed hybrid synchronization method begins with a non-coherent synchronization mechanism based on energy detection using On-Off Keying (OOK) modulation to coarsely synchronize the receiver by determining the correct integration window in which the received signal resides. Once the coarse synchronization level is achieved, a coherent template-based coherent correlation employing Binary Phase-Shift Keying (BPSK) modulation is carried-out for fine synchronization and to benefit from coherent payload decoding.

A prototype IR-UWB receiver operating from 3.5 to 5 GHz has been implemented in a TSMC 65 nm CMOS technology. Our proposed receiver architecture enabled us to compare our hybrid synchronization approach to two common receiver architectures, namely non-coherent energy detection and coherent detection receivers.

The receiver architecture utilizes a self-mixer for a non-coherent detection based on OOK modulation and a template correlation for a coherent detection based on BPSK modulation. Most blocks in the proposed receiver architecture, including the LNA, mixer and baseband circuitry are shared between the non-coherent and coherent modes to minimize the total power consumption and receiver area. A two-step coarse and fine acquisition mechanism is utilized to simplify the coherent synchronization and minimize the total required packet length. A multi-resolution Delay-Locked Loop (DLL) and a fast start-up Voltage Controlled Oscillator (VCO) provide the proper phase for the integration window and template generation.

The receiver consumes 6.8 mW in non-coherent mode and 8.8 mW in coherent mode when operating fully ON, excluding the power consumption of the buffers and the digital baseband processor. It achieves a -68 dBm, -70.5 dBm, and -70.8 dBm RF sensitivity at a 10^{-3} BER in

the non-coherent, coherent, and proposed hybrid mode, respectively. Our proposed receiver architecture, in combination with the hybrid coherent synchronization algorithm, demonstrates that the proposed synchronization approach is capable of significantly reducing the overhead incurred by the preamble. The packet duration is reduced from 37.12 μs in the solely coherent template correlation to 24.42 μs with the proposed hybrid synchronization method for a 1024-bit payload.

Keywords: Ultra-wideband, impulse radio, coherent, non-coherent, synchronization, low pow, template-based correlation

TABLE OF CONTENTS

Page

LIST OF FIGURES

LIST OF ABBREVIATIONS

ADC	Analog to Digital Converter
BER	Bit Error Rate
bps	bits per second
BPSK	Binary Phase Shift Keying
DAC	Digital to Analog Converter
Eb/N0	bit energy / noise power spectral density
EIRP	Equivalent Isotropically Radiated Power
DLL	Delay Locked Loop
EIRP	Equivalent Isotropically Radiated Power
FCC	Federal Communications Commission
BFSK	Binary Frequency Shift Keying
IoT	Internet of Things
IR-UWB	Impulse Radio Ultra Wideband
LNA	Low Noise Amplifier
NF	Noise Figure
OOK	On-Off Keying
PLL	Phase Locked Loop
PPM	Pulse Position Modulation
RF	Radio Frequency

RMS	Root Mean Square
SNR	Signal-to-Noise Ratio
S-OOK	Synchronized On-Off Keying
TR	Transmitted Reference
UWB	Ultra-Wideband
VCO	Voltage Controlled Oscillator
PRF	Pulse Repetition Frequency

LIST OF SYMBOLS AND UNITS OF MEASUREMENTS

A	ampère
mA	mili-ampère
μA	micro-ampère
V	volt
mV	mili-volt
μA	micro-volt
W	watt
mW	mili-watt
μW	micro-watt
nW	nano-watt
s	second
ms	mili-second
μs	micro-second
ns	nano-second
Ω	ohm
F	Farad
Hz	Hertz

INTRODUCTION

IR-UWB technology is expected to meet the ever-increasing demand for high data rates, low latency, and low power consumption because of its attractive features. It has recently gained a lot of attention for consumer electronics applications and wearable low-power sensor nodes. Rather than transmitting a very high power narrow band continuous signal in conventional narrowband transceivers, IR-UWB sends and receives very short pulses in time. These short pulses allow the energy to spread over a wide frequency range. In addition, since these pulses are very short in duration, the transmitter and receiver can be duty cycled to minimize power consumption. As a result, it is a suitable solution for high data rate wireless transfer and short-range communication at low power consumption.

Motivation

Since the late 2000s, researchers have used coherent and non-coherent energy detection techniques to design low-power receiver topologies and IR-UWB transceivers for low-power applications. Non-coherent energy detection transceivers usually offer cost-effective solutions with their simple energy detection architecture. In spite of their simple architecture, they are unable to provide good receiver sensitivity and interference immunity.

A coherent system, on the other hand, provides a more robust link and better receiver sensitivity. The flexibility of fully digital coherent transceivers is one of their advantages. A fully digital transceiver, however, consumes a lot of power due to high sample rates Analog to Digital Converter (ADC) and matched filters. With template correlation coherent receivers, the signal correlation can be moved into the analog domain, which can reduce the power consumption of fully coherent receivers. Despite this, synchronizing narrow IR-UWB pulses with received pulses becomes challenging.

An integrated coherent and non-coherent receiver architecture is proposed in this study. The power consumption and energy efficiency of coherent receivers can be reduced as a result.

Contributions

The main contributions of this thesis are described in the following subsections.

A Low-Power Agile Coherent IR-UWB Receiver with Non-Coherent-Assisted Synchronization

An agile IR-UWB receiver architecture based on a template-based correlation utilizes a novel hybrid synchronization based on a non-coherent assisted synchronization algorithm in order to improve the energy efficiency of the receiver. A coarse level synchronization is achieved by first selecting the best integration window covering the maximum amount of signal energy. The receiver utilizes a self-mixing approach to achieve a coarse level synchronization. The receiver can then use the pre-synchronized state to perform a coherent synchronization search using a template-based correlation synchronization by sliding the template over the search area. This work is implemented in a 65 nm CMOS technology. Chapter 3 will provide a more detailed discussion.

The contribution associated with this system is the following submitted paper and represents my main work:

A. P. kakhki, M. Taherzadeh and F. Nabki, "A Low-Power Agile Coherent IR-UWB Receiver with Non-Coherent-Assisted Synchronization," manuscript submitted to the IEEE Transactions on Circuits and Systems I: Regular Papers, December 2022.

The following two contributions are not my main thesis work but are listed here and briefly described. These are the fruit of a collaboration with N. Shams and for which I contributed to significant portions of the circuitry and its testing.

Reconfigurable IR-UWB Current Mode Switched Receiver for IoT Applications. (Shams, Kakhki & Nabki (2019))

The Low Noise Amplifier (LNA) is the first block of any receiver after the antenna that provides signal amplification with minimal degradation of the Signal-to-Noise Ratio (SNR). Since the Noise Figure (NF) of the receiver is dominated by the NF of the LNA, it is a critical block in the receiver front-end. Also, the impact of noise contributions from all subsequent stages will be reduced by the LNA. In order to maximize power transfer, the input matching of the LNA must be kept good enough over the frequencies of the band of interest.

In this work, a fully differential multi-band impulse radio receiver based on a non-coherent architecture that includes a differential reconfigurable LNA, a squarer circuit and variable gain amplifiers were implemented.

The contribution associated with this LNA is done jointly with N. Shams in the following paper : N. Shams, **A. P. kakhki** and F. Nabki, "Reconfigurable IR-UWB Current Mode Switched Receiver for IoT Applications," 2019 26th IEEE International Conference on Electronics, Circuits and Systems (ICECS), 2019, pp. 9-12, doi: 10.1109/ICECS46596.2019.8965095.

An OOK and Binary FSK Reconfigurable Dual-Band Non-Coherent IR-UWB Receiver Supporting Ternary Signaling

The receiver architecture proposed in this work provides multi-modulation supports with ternary signaling. The designed receiver can operate in different scenarios such as three different single bands and multi-band from 3-6 GHz. Thanks to the proposed multi-band LNA and the concurrent dual-band receiver architecture, the receiver can distinguish between the bands of the received signal and performs Binary Frequency Shift Keying (BFSK) demodulation. A chip micrograph of this work designed and fabricated in TSMC 130 nm CMOS technology is shown in Fig. 0.1.

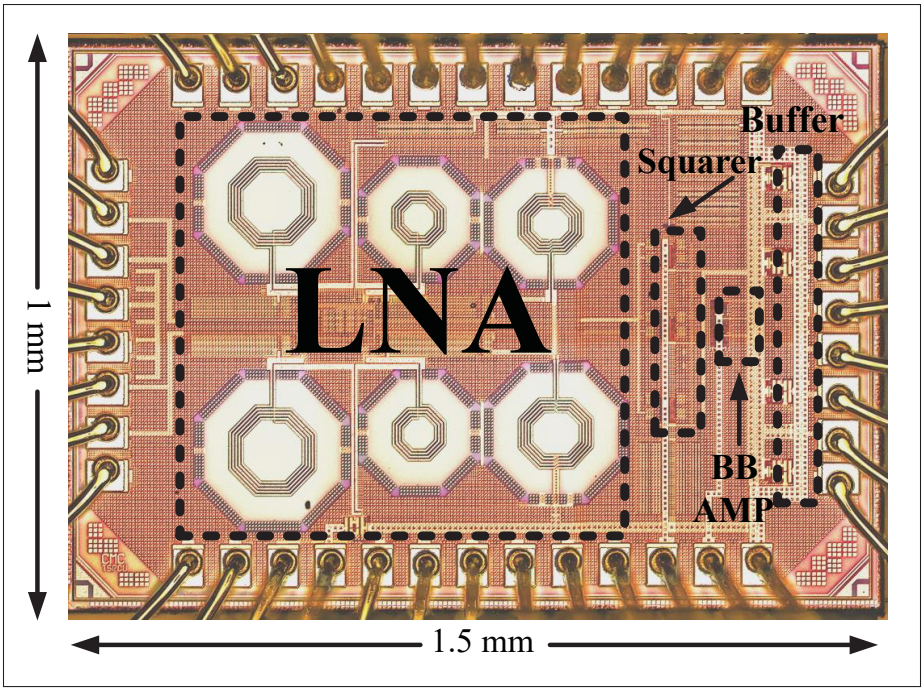

Figure 0.1 Micrograph of the reconfigurable IR-UWB receiver front-end.

The contribution associated with this work where I collaborated with N. Shams is detailed in the following paper :

N. Shams, **A. P. kakhki**, M. Nabavi and F. Nabki, "An OOK and Binary FSK Reconfigurable Dual-Band Non-Coherent IR-UWB Receiver Supporting Ternary Signaling," manuscript submitted to the IEEE Transactions on Very Large Scale Integration, October 2022.

Thesis Outline

This thesis is organized as follows:

Chapter 1 presents background information on IR-UWB communication systems. IR-UWB systems will be discussed in terms of their advantages and disadvantages. A discussion will also be given on the different modulation techniques.

Chapter 2 presents some related state-of-the-art literature and studies. There will be a discussion of some recent non-coherent receiver architectures, namely energy detection and peak detection, as well as coherent detection, namely digital and analog correlation. This chapter will also discuss different synchronization techniques used in these types of receivers.

Chapter 3 presents the manuscript of the submitted journal paper entitled "A Low-Power Agile Coherent IR-UWB Receiver with Non-Coherent-Assisted Synchronization".

Finally, a conclusion and discussion are presented in the last chapter, including recommendations for future research and improvements.

A brief discussion of the number of tested chip is included in an appendix at the end of this thesis.

CHAPTER 1

BACKGROUND

This chapter presents some background for the IR-UWB systems presented in this thesis.

1.1 Impulse Radio Ultra-Wideband

Unlike narrowband communication systems which employ a specific continuous carrier signal to transmit information in different modulations, IR-UWB systems use short-duration electromagnetic pulses in the order of a few nanoseconds for data transmission and reception. Since the IR-UWB pulses are short in time, they occupy large bandwidth, typically in the order of hundreds of MHz and up to a few GHz of bandwidth.

An IR-UWB transmitter has a very low power spectral density because its energy is sent across a wide range of frequencies which are occupied by other radio systems. In 2002, the Federal Communications Commission (FCC) allowed the unlicensed use of the UWB spectrum. In accordance with part 15 of FCC, any transmission that has at least 500 MH -10 dB bandwidth or 20 % of fractional bandwidth is considered a UWB transmission(Commission (2002)). A range of 3.1 to 10.6 GHz was specified for UWB transmission by the FCC. Additionally, the FCC also determined the maximum allowable emission power with an average of -41.3 dBm/MHz (75 nW/MHz) Equivalent Isotropically Radiated Power (EIRP). European Telecommunications Standards Institute (ETSI), mainly for Europe, mandated slightly different regulations from those required by the FCC. Other countries have also followed suit with their own UWB regulations, which are usually inspired by the FCC or ETSI.

1.2 UWB: Advantages and Disadvantages

It is one of the key advantages of UWB systems that they can potentially occupy a large bandwidth, up to 7.5 GHz. According to Shannon's information theory, the maximum information transmission rate over a Additive White Gaussian Noise (AWGN) channel can be

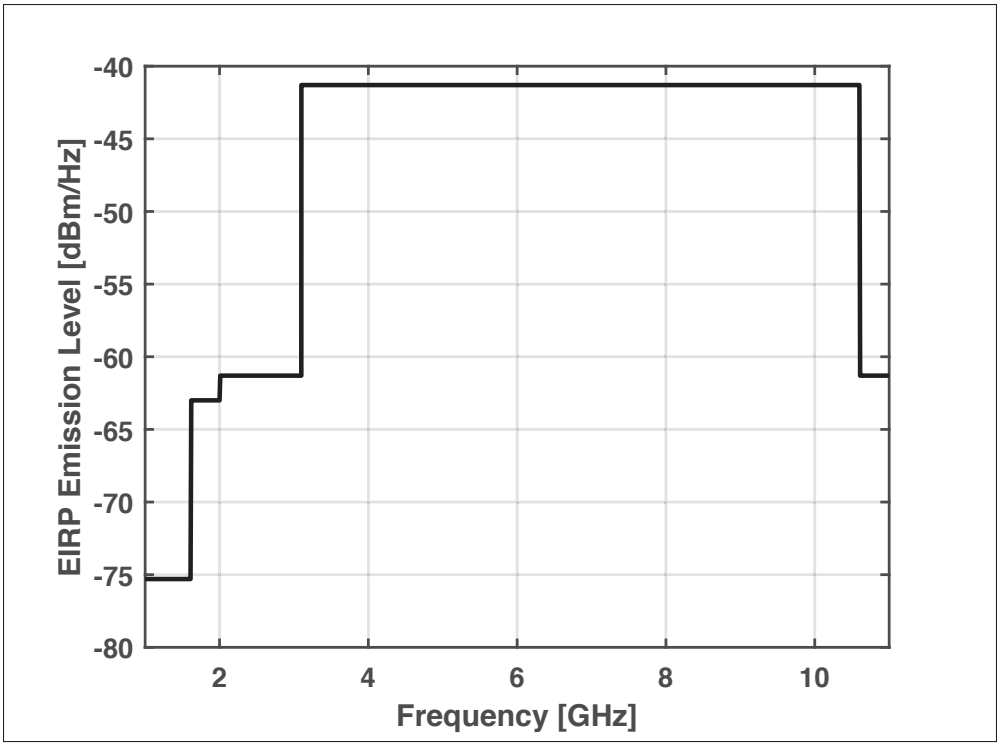

Figure 1.1 FCC spectral mask for UWB communications
Taken from Phan *et al.* (2008).

defined as:

$$C = Blog(1 + \frac{S}{N}). \tag{1.1}$$

where C is the maximum channel capacity (bps), B is the channel bandwidth (Hz), and S/N is the SNR, signal-to-noise ratio. It can be seen that the upper limit of the channel capacity increases proportionally with bandwidth, while it increases logarithmically with SNR.

Additionally, IR-UWB systems can be implemented with low complexity and low-cost architectures. The simplicity of IR-UWB systems arises from the wideband nature of the signal transmission and reception which relaxes requiring highly accurate signal generation. To generate highly accurate signals, narrowband communication systems usually rely on high-frequency synthesizers that consume large amounts of energy. Unlike narrow band communication systems, IR-UWB systems can operate with a cheap, low-cost crystal oscillator. This can drastically reduce the power consumption of the IR-UWB systems and extend the operating life

of a battery-operated communication system. This requires careful design, however, as some commercial implementations of IR-UWB are not considered to be low power (SRM,DW1).

Furthermore, the UWB systems share the spectrum with other existing communication systems. Since the transmitted average power of UWB systems is low compared to other narrowband communication technologies such as Bluetooth and WiFi, they are less likely to be intercepted, which makes them a promising solution for highly secure communication and military applications (IEEE 802.15.4z (2020), Fontana (2004)). Also, UWB systems are unlikely to interfere with other communication systems, which allows coexistence with current communication systems.

Ultra-wideband technology benefits primarily from the use of excess bandwidth. There are, however, some consequences associated with this. Performance degradation is a major challenge for ultra-wideband systems because of their high bandwidths, which allow more noise to affect the receiver. This will result in a decrease in receiver sensitivity. In addition, IR-UWB systems receive more out-of-band interference than narrowband systems due to their wide bandwidth. Therefore, careful consideration for having enough out-of-band rejection needs to be taken into account.

The low power spectral density of UWB systems prevents interference with other communication systems. However, it is not necessarily reciprocal. Other existing high-power narrowband systems can interfere with the UWB systems and easily corrupt the UWB signal. In addition, high-power narrowband signals can desensitize receivers if they are not properly filtered. In order to reduce narrowband blocker effects on UWB systems, proper frequency allocation is necessary.

Furthermore, UWB systems are usually capable of offering high-speed data transmissions. In other words, the period of time between the "0"s and the "1s" are shortened as a result of their large bandwidth. UWB systems are also benefitted from their large bandwidth to be less affected by multi-path channels, requiring less fading margin (Kang & Kim (2012)).

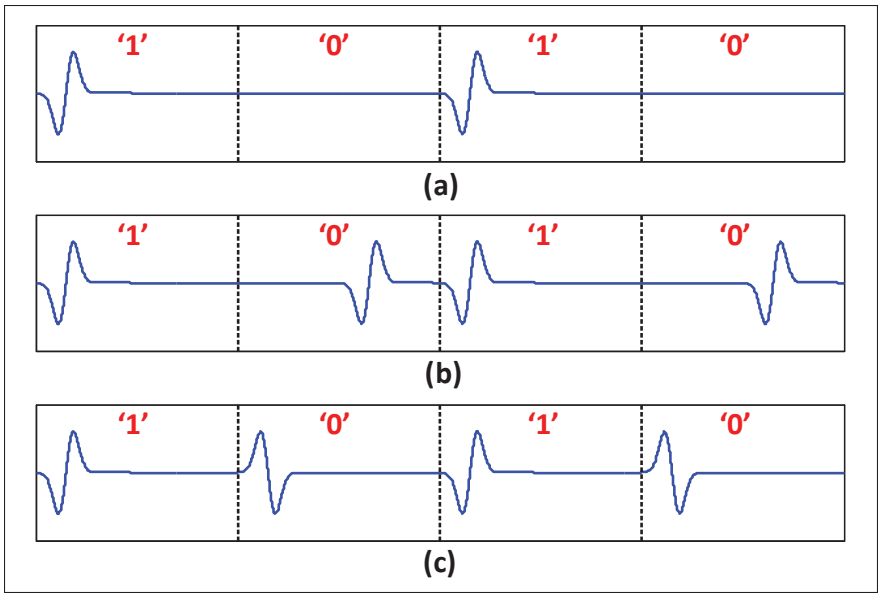

Figure 1.2 Different modulation waveforms: (a) OOK, (b) PPM and (c) BPSK
Taken from Allidina (2015).

To ensure that transmitted data is properly received, it is necessary for the receiver to be synchronized with the transmitted pulse. Due to their short duration and low power, the initial detection and synchronization of the pulses are difficult, and this topic is a key aspect tackled in this thesis, notably with regard to improving the energy consumed while synchronizing a frame.

1.3 Modulation Techniques

IR-UWB systems use a sequence of pulses to convey information. Different modulation techniques can be used in an IR-UWB system such as OOK, Pulse Position Modulation (PPM) and BPSK. In the most straightforward format, also known as OOK modulation, the presence or absence of a pulse represents a data bit "0" or “1”, respectively. A ’1’ or a ’0’ is transmitted depending on where the pulse falls within a symbol frame in PPM modulation. In BPSK, the data is encoded in the phase of the transmitted pulse. Figure. 1.2 illustrates how data is modulated in these modulations.

In the OOK modulation scheme, a transmitter is only required to send a pulse when the data is ‘1’. While in the PPM and BPSK, it should send a pulse for every bit. As a result, PPM and BPSK require less output power to meet emission regulations as OOK modulation can be designed to only require 50 percent of the symbols requiring emitted energy. Therefore, for the same transmitted bitstream, each pulse in the OOK format can have twice the power of the pulses in PPM and BPSK, while still meeting the average allowable power requirements.

A BPSK system, however, has an inherent 3-dB sensitivity advantage over an OOK or a PPM system. This is due to the fact that the signal constellation distance of BPSK modulation is double that of OOK and PPM modulations. The phase pseudo-randomness can also mitigate the discrete spectral lines in the PSD of an OOK or PPM pulse modulation. BPSK modulation, however, does require a coherent receiver, which is a complex and energy-intensive way to detect the transmitted data.

CHAPTER 2

LITERATURE REVIEW

A summary of the related literature and studies is presented in this chapter. This chapter also discusses different IR-UWB receiver implementations, including coherent and non-coherent receiver architectures.

2.1 Non-coherent detection

Non-coherent detection can be categorized into different subcategories. In non-coherent receivers, energy detection, peak detection, and super-regenerative architectures (Thoppay, Dehollain, Green & Declercq (2011)) are well-known receiver architectures.

In energy detection receivers, the pulse's energy is measured over a period of time. In contrast, peak detection receivers are based on detecting the amplitude value of the incoming signal. For energy detection and peak detection methods to be effective, multi-stage RF amplifiers are usually required so that the received signal can be amplified. In contrast to super-generative receivers, where the RF amplification constraint is not as high as in energy detection and peak detection receivers, this results in higher power consumption. However, energy detection and peak detection receivers provide a more linear and reconfigurable front end with much less RF leakage than super-generative receivers.

2.1.1 Energy detection

In order to measure the energy of the received signal, a mixer and an integrator are traditionally used as part of the energy detection process. A mixer is used to self-mix and down-convert the received signal after it has been received and amplified by the LNA and RF amplifiers. An integrator is then used to estimate the pulse energy by accumulating the signal power over a certain period of time.

A low complexity implementation and low power consumption are the primary motivations for non-coherent receivers. Most non-coherent receivers do not require highly accurate timing and synchronization. As a result, they can rely on low-power crystal oscillators. In spite of this, non-coherent architectures do not provide superior RF performance since the noise will be self-mixed and integrated in addition to the received signal. Therefore, non-coherent receivers do not offer optimal RF performance when compared with coherent receivers.

A three-channel receiver with a frequency range of 3 to 5 GHz is proposed in (Daly, Mercier, Bhardwaj, Stone, Aldworth, Daniel, Voldman, Hildebrand & Chandrakasan (2010)) for insect flight control. Since the flight control receiver should be located on the insect, the wireless receiver is one of the most critical electronic components in this system. This results in tight restrictions on its volume and weight. A non-coherent energy detection method is selected to take advantage of low power consumption, thereby avoiding heavy batteries and increasing the system's lifetime without any battery replacement.

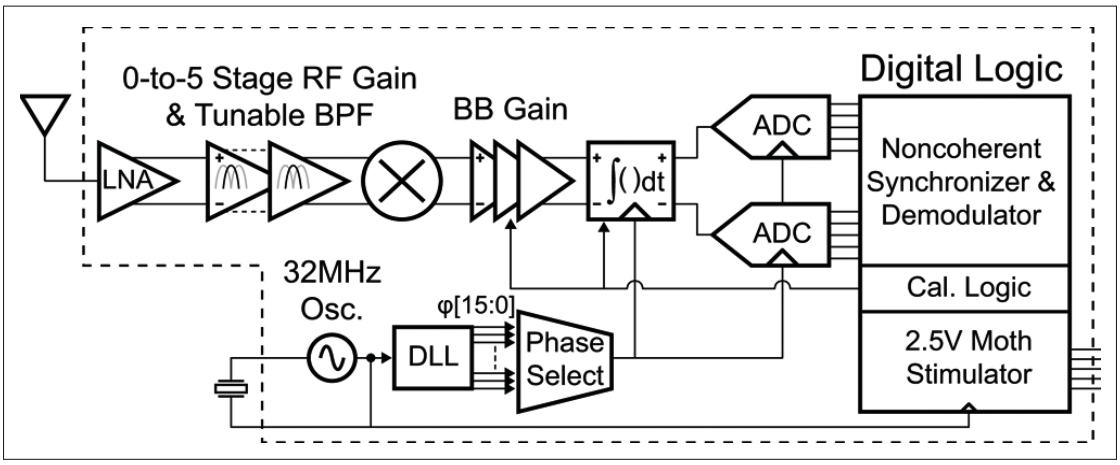

Figure 2.1 A simple and lightweight IR-UWB receiver SoC for an Insect Motion Control using a non-coherent approach
Taken from Daly *et al.* (2010).

The designed receiver can operate at 16 Mbps as its maximum data rate while supporting OOK and PPM modulation for the 802.15.4a wireless standard. The block diagram of the receiver is shown in Fig. 2.1. In order to minimize the digital noise introduced by the digital circuits, a differential architecture is chosen over a single-ended architecture. An LNA based on a

common-gate, common-source (CG-CS) LNA structure followed by up to five variable RF gain stages provides signal amplification and reduces the effect of the noise of the subsequent stages on the overall RF performance of the receiver. Non-coherent energy detection receiver architectures also require significant gain amplification before the self-mixer. A self-mixer after the RF amplifiers facilitates down-converting the signal to the baseband by implementing a self-mixing approach.

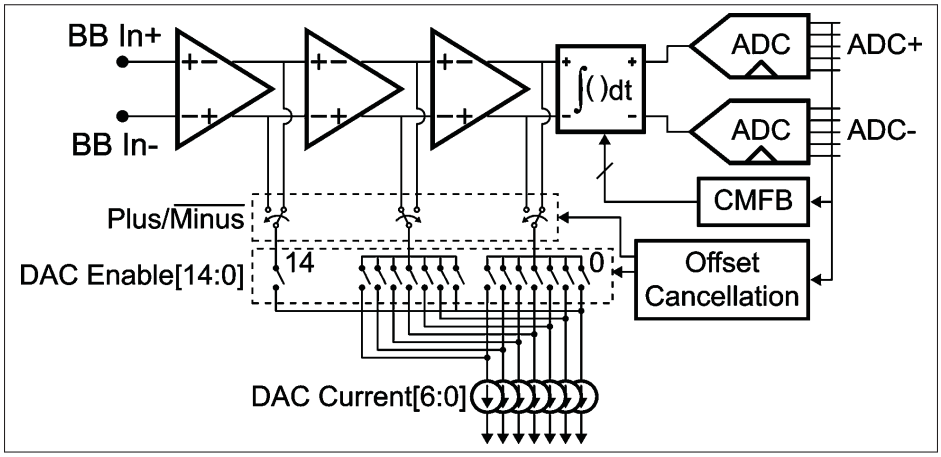

Figure 2.2 Baseband signal chain and offset cancellation loop
Taken from Daly *et al.* (2010).

A baseband (BB) gain stage also introduces BB amplification after the signal has been down-converted. Simulation results show an 83 V/V and 3 dB bandwidth of 230 MHz in the baseband stages. Since the gain is relatively high and the input signal of the baseband amplifier is too low, careful offset compensation is required for the baseband circuit. A digitally controlled current mode Digital to Analog Converter (DAC) is utilized to compensate for the amplifier offset, as shown in Fig. 2.2.

After the BB amplifier stages, an integrator is used to measure the energy of the signals in a specific window of time. A parallelized ADC/integrator structure is used for synchronization. Baseband signals are digitized into digital form by two ADCs, so they can be further analyzed by a baseband processor. The receiver requires an off-chip oscillator operating at a fixed 32 MHz clock. Different clock phases are provided by the DLL for the integration window and the

ADC. The BB gain setting and the correct DLL phase for the integration window are set through the synchronization loop.

2.1.2 Peak Voltage Detection

In non-coherent receivers, peak detection is another approach. An energy detection IR-UWB receiver measures the energy of the received pulse within a window, while a peak detection receiver measures the signal's instantaneous peak value. Despite the fact that peak detection is more likely to make incorrect decisions in noisy environments, the noise will not accumulate as it does with energy detection (Allidina (2015)).

A non-coherent receiver in the 3.1-4.9 GHz band is proposed in (Vauche, Muhr, Fourquin, Bourdel, Gaubert, Dehaese, Meillere, Barthelemy & Ouvry (2017)), which has a pulse shaping technique on the transmit side and a Peak Voltage Detection (PVD) on the receive side. The block diagram of the receiver architecture can be seen in Fig. 2.3.

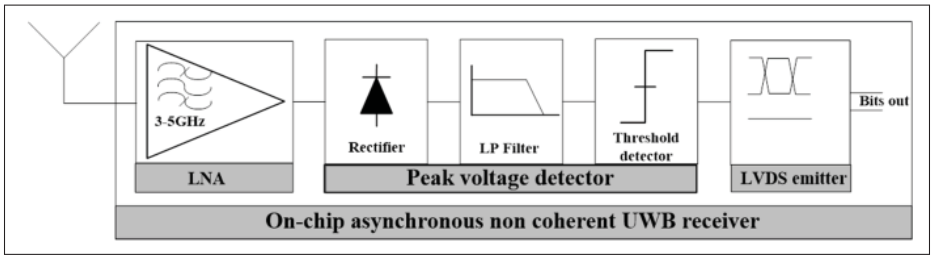

Figure 2.3 A peak voltage detection IR-UWB receiver
Taken from Vauche *et al.* (2017).

Peak detection eliminates the need for conventional gain RF stages, one of the most power-consuming parts of any receiver's front end. The BER for peak voltage detection using an OOK modulation system for AWGN channels is estimated. Figure 2.3 illustrates that PVD requires greater input power at the receiver to achieve the same BER as energy detection (ED). Thus, only very short-range communication could be achieved with this approach. Therefore, PVD does not appear to be an interesting alternative.

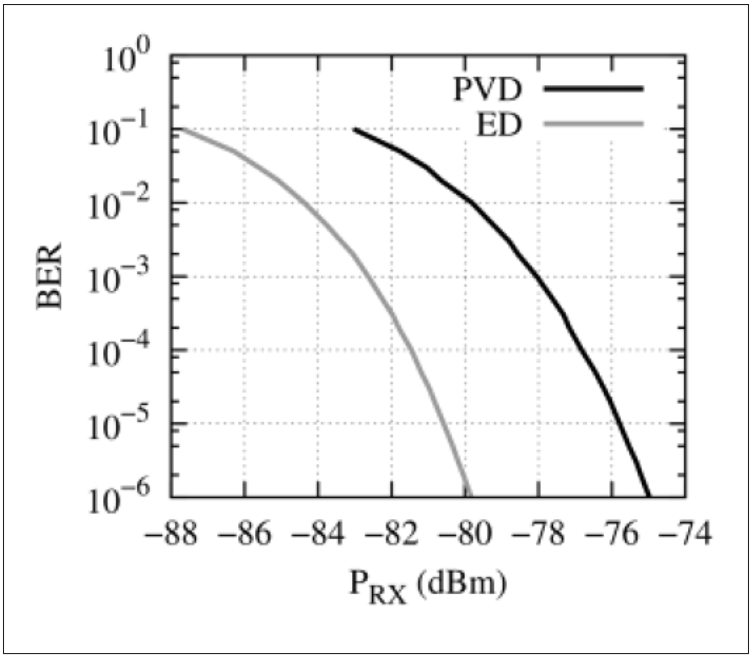

Figure 2.4 BER waterfall curves for a PVD and energy detection receiver Taken from Vauche *et al.* (2017).

According to (Vauche *et al.* (2017)), the designed PVD receiver's sensitivity is -85 dBm at 1 Mbps. At 100 Mbps, the receiver consumes 30.5 mW, which translates into a power efficiency of 0.305 nJ/b. Though it might appear intuitively that PVD would perform better than ED in noise and multipath-dominated channels (Allidina (2015)), PVD's RF performance in AWGN channels is not as good as ED's, as shown in Fig. 2.4.

2.2 Coherent Detection

An optimal coherent receiver is able to decode the absolute phase information of the received carrier-modulated signal. As opposed to this, a non-coherent energy detection receiver can only detect the energy of the signal it receives, and it is unable to retrieve the phase information. Coherent receivers can be implemented in an analog or a digital correlation fashion. The following sections provide examples of each method.

2.2.1 Digital Correlation

In (Chandrakasan, Lee, Wentzloff, Sze, Ginsburg, Mercier, Daly & Blázquez (2009)), a partial rake receiver architecture is proposed. The RF front end is based on direct conversion that uses an I/Q receiver architecture, as shown in Fig. 2.5. First, an LNA amplifies the received signal. The image of the signal is then removed with an image rejection filter. The signal is then down-converted into the I/Q path, where the ADCs digitize each path for acquisition and demodulation by the baseband processor.

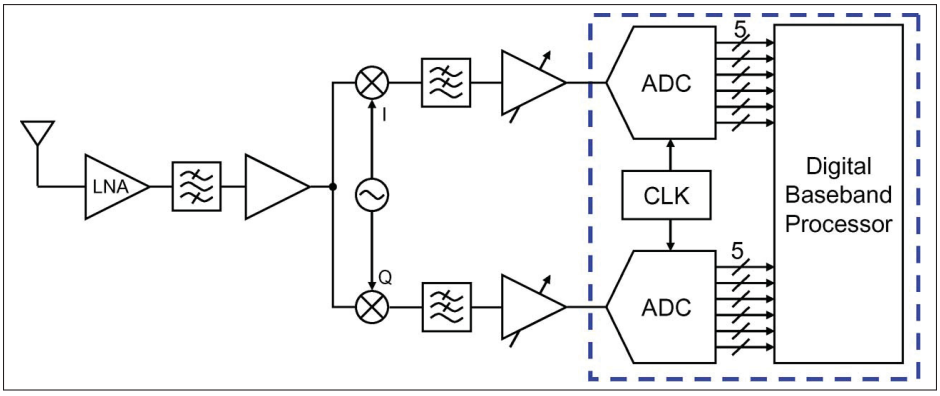

Figure 2.5 A direct conversion UWB receiver architecture for high-data-rate systems
Taken from Chandrakasan *et al.* (2009).

In (Zheng, Arasu, Wong, The, Suan, Tran, Yeoh & Kwong (2008)), an 802.15.4a IEEE-compliant UWB transceiver that can operate over 12 channels in the UWB spectrum from 3-9 GHz in 0.18 μm CMOS technology is presented. The proposed architecture can decode a BPM-BPSK modulation and achieves a -75 dBm RF sensitivity with an overall 6.51 nJ per pulse energy consumption at the receiver side.

Coherent receivers with a digital correlation implementation usually offer superior RF performance. Their power consumption, however, is typically high. Although the power consumed by the digital circuits and leakage current can be reduced by going to advanced CMOS process nodes, they are still not well-suited to low-power applications since they require highly accurate timing and consume a significant amount of power for synchronization.

2.2.2 Analog Template-based Correlation

There is another type of coherent receiver that uses analog correlation (template-based correlation) for its operation. This type of receiver can significantly relax the ADC constraints (Nyquist rate) by correlating the received signal with a known template in the receiver. Correlations can be performed in the RF as well as the IF/BB domains. A comparison of the normalized correlation value in BB and RF is shown in Fig. 2.6. A BB correlation requires that the input signal be down-converted, which results in the loss of phase information. Therefore, non-coherent modulations such as OOK and PPM are better suited to BB correlation.

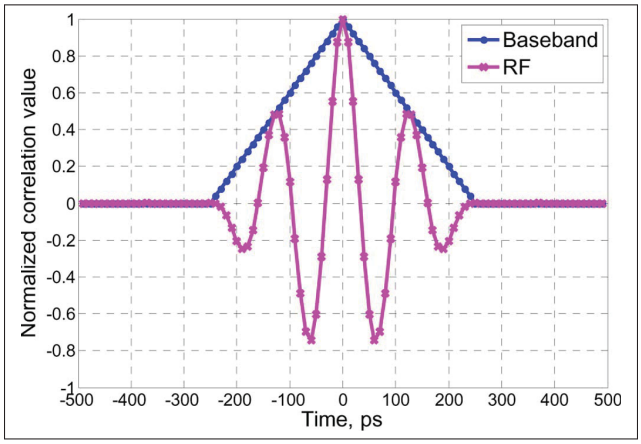

Figure 2.6 Auto-correlation function comparison.
Taken from Zhou *et al.* (2011).

A high level of accuracy is required for template generation and synchronization in order to achieve RF correlation. A 30 ps mismatch error for instance in template synchronization introduces a 10 percent error for correlation at the BB but complete degradation for correlation at the RF.

The block diagram of the designed coherent system based on RF correlation can be seen in Fig. 2.7. The triggering pulse of the template generation can be controlled by a timing synchronizer block. By using a digital time control circuit as opposed to delaying a IR-UWB

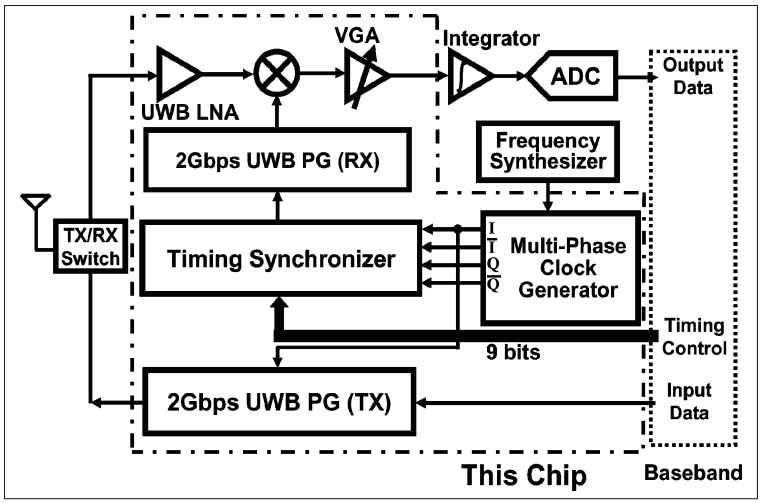

Figure 2.7 IR-UWB transceiver architecture.
Taken from Zhou *et al.* (2011).

pulse, which is not as straightforward as in the digital domain, the trigger of the template generator could be delayed in the digital domain instead.

BB analysis will monitor how well the template matches the incoming pulse and will be adjusted after demodulating the previous pulse. This process can be achieved during the acquisition time. Afterwards, data communication is carried out.

It also shows that the template can be either the exact transmitted pulse or a sinusoidal wave using a local oscillator in order to have a simpler architecture. This is at the cost of performance degradation. A 3 dB performance will be lost using a local oscillator, as shown in Fig. 2.8.

2.3 Synchronization

Proper symbol demodulation requires the receiver and transmitter to be synchronized, not only in frequency but also in time. In other words, the transmitter and receiver should be able to predict when they are expecting to receive some data from each other. In IR-UWB transceivers, this task is even more critical since both transmitter and receiver are kept off between frames to conserve power.

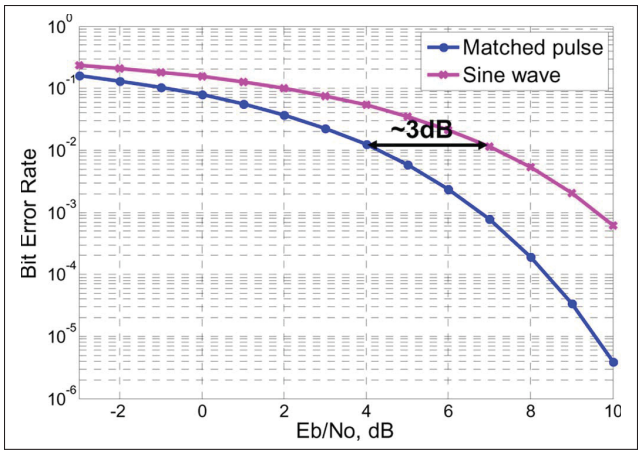

Figure 2.8 SNR degradation with different template shapes. Taken from Chandrakasan *et al.* (2009).

As discussed, all the synchronization is also pushed into the digital domain and demodulation is carried out using digital correlators in digital correlation receivers. In (Chandrakasan *et al.* (2009) and Zheng *et al.* (2008)), the BB processor takes the I/Q digitized data from the ADC and tries to find a known pattern using auto/cross-correlation functions. This usually requires huge correlator banks which consume a huge amount of power and area. Also, since the correlator banks are huge, the leakage power of the digital BB processor becomes a challenge in these types of receivers as they need so many digital gates.

An Ultra-Wide Band (UWB) packet consists of a preamble and a payload, as shown in Fig. 2.9. In the preamble section, a 31-bit golden code that has desirable auto-correlation properties is repeated during the receiver synchronization.

The baseband processor shown in Fig. 2.10 employed 620 correlators as the matched filter bank in 5 fingers and consumed 7 mW and 1.7 mW, respectively, for acquisition and demodulation, while operating at 0.4 Volts. The receiver can achieve a high data rate of 100 Mb/s using BPSK and a low data rate of 16.7 Mb/s using PPM modulation.

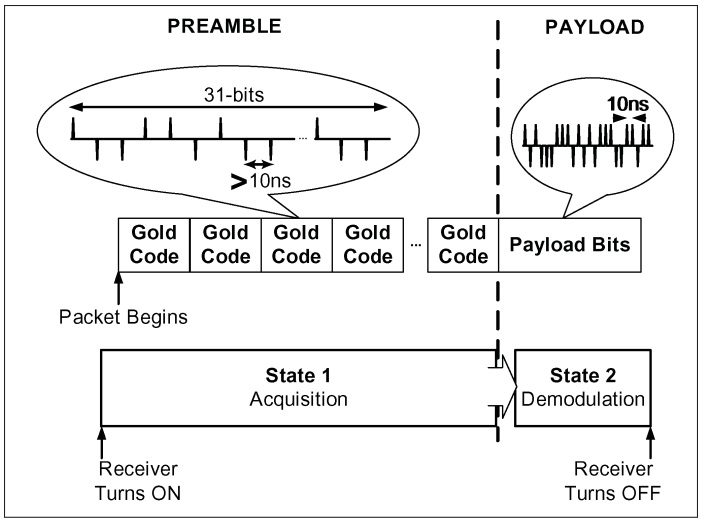

Figure 2.9 UWB packet structure
Taken from Chandrakasan *et al.* (2009).

It is noted that in a fully digital correlation-based receiver, the RF front end is kept simple, and signal correlation is handled digitally. Such a transceiver offers flexibility and scalability as its main advantages. However, its power consumption is usually dominated by the high power consumption ADC and the matched filter banks. Moreover, since the sampling rate of the ADC needs to be at least twice the signal bandwidth and is usually in the range of several GHz, it becomes another overhead in power consumption. In analog correlation coherent receivers, since there is a template being generated in the receiver that needs to be synchronized with the received signal, the synchronization task is to find the phase for the template generator. Instead of delaying an IR-UWB signal which is not trivial, the trigger of the template generator, which is a digital signal, can be delayed. (Zhou *et al.* (2011)). In order to find the proper phase for the template generator, all the positions within a symbol need to be searched. This can become challenging if the search space is too wide. In other words, if the symbol time is too long, a very long preamble is needed at the beginning of a packet so that the receiver has enough time to search the symbol time, which can be an overhead in the overall energy consumption per bit.

In non-coherent detection receivers, on the other hand, the synchronization task is mainly to find the proper integration window in which the signal energy resides (Daly *et al.* (2010)). This is

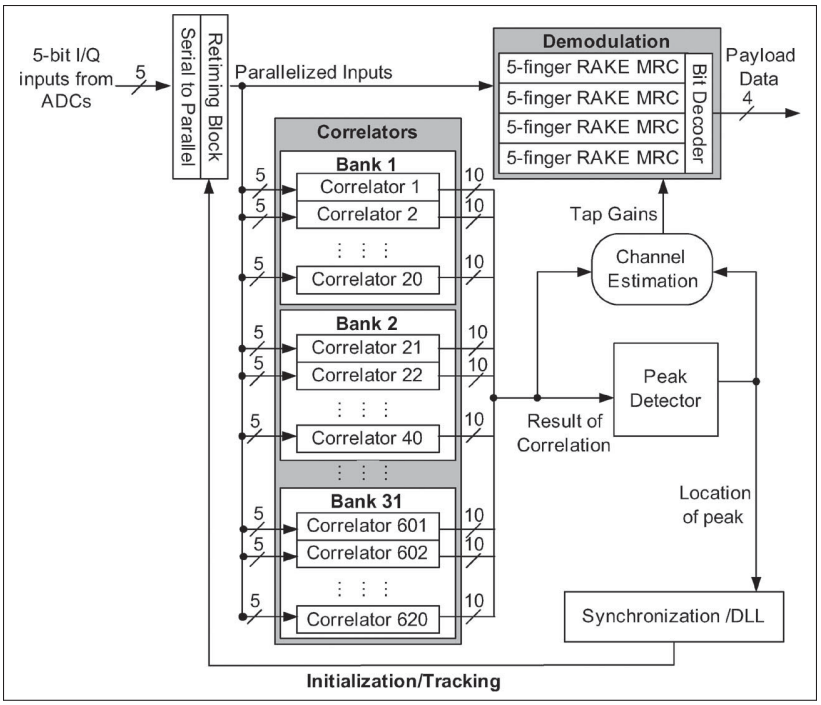

Figure 2.10 Digital baseband processor in digital correlation receivers.
Taken from Chandrakasan *et al.* (2009).

not usually as challenging as it is in coherent receivers since accurate synchronization between the transmitter and receiver is more relaxed in non-coherent structures. As a result, the preamble overhead needed for synchronization is not as significant. A synchronized-OOK (S-OOK) modulation scheme is proposed in (Crepaldi, Li, Fernandes & Kinget (2011)) to minimize the synchronization time and reduce the average power consumption of a non-coherent receiver. Although this technique achieves fast synchronization, it is not an optimal solution in terms of energy consumption per bit, as synchronization has to happen for every bit.

Further analysis and details for synchronization approaches and algorithms will be given in Chapter 3.

2.4 Conclusion

A review of some related works on IR-UWB receivers utilizing different detection and synchronization mechanisms, including energy and peak voltage non-coherent receivers as well as analog and digital correlation coherent receivers, was presented in this chapter. The non-coherent receivers based on energy detection suffer from low sensitivity, especially in noisy environments, resulting in a degradation in BER performance. Nevertheless, these structures allow for simple low-power implementations, which is desirable in ultra-low-power systems. A peak voltage detection receiver was shown to achieve lower power consumption as it does not require power-hungry RF gain stages, but it showed lower sensitivity than energy detection receivers, making them suitable for a very limited set of applications.

On the other hand, a coherent receiver outperforms a non-coherent receiver in terms of RF performance. However, coherent detection implementations require high power blocks to ensure accurate synchronization. Coherent receivers can be implemented in either analog or digital correlation fashions. One of the significant drawbacks of digital architecture receivers is their complex synchronization approaches. Moving the correlation into the analog domain can mitigate the complexity of the synchronization requirement in the coherent receivers. However, these receivers still are quite sensitive to synchronization accuracy and thus require a significant amount of time for synchronization.

The next chapter will describe a hybrid receiver architecture and a novel synchronization algorithm that benefits from both non-coherent and coherent receivers. For non-coherent detection, an energy detection method was selected over peak voltage detection in order to achieve improved RF sensitivity. To reduce the complexity of the system, an analog correlation method based on template-based correlation is selected over digital correlation. A novel synchronization algorithm is also provided in order to synchronize the proposed system and reduce the energy cost of the synchronization.

CHAPTER 3

A LOW-POWER AGILE COHERENT IR-UWB RECEIVER WITH NON-COHERENT-ASSISTED SYNCHRONIZATION

Amin Pourvali Kakhki[1] , Mohammad Taherzadeh[2] , Frédéric Nabki [1]

[1] Department of Electrical Engineering, École de Technologie Supérieure,
1100 Notre-Dame Ouest, Montréal, Québec, Canada H3C 1K3
[2] Department of Electrical Engineering, Ferdowsi University of Mashhad, Iran

Paper submitted to the IEEE Transactions on Circuits and Systems I: Regular Papers

Abstract

This paper presents a non-coherent assisted synchronization mechanism for coherent IR-UWB receivers. A two-step coarse and fine acquisition mechanism is utilized to simplify the coherent synchronization and minimize the total required packet length. This hybrid scheme reduces the total power consumption of the receiver. The reception of a UWB packet begins with an energy efficient non-coherent synchronization portion in OOK modulation non-coherent acquisition. This reduces the search space for the coherent reception by first finding the best integration window that has the most energy of the received signal. Afterwards, the receiver searches coherently in BPSK modulation within only the pre-selected integration window instead of the whole symbol time. Self-mixing and template-based correlation are utilized for the non-coherent and coherent reception, respectively. Most of the front-end blocks are shared between the coherent and non-coherent modes, including the LNA, mixer, and the baseband circuitry that follows to minimize the total power consumption of the receiver. A differential architecture including a LNA, a mixer, a fast start-up template generator, an integrator, and a differential comparator are utilized for the receiver front-end. A prototype of the proposed receiver operating from 3.5 to 5 GHz over four bands, each spaced by 500 MHz, is implemented in 65-nm CMOS technology. The proposed receiver architecture achieves a -68 dBm, -70.5 dBm, and -70.8 dBm sensitivity at a 10^{-3} BER at 50 MHz Pulse Repetition Frequency (PRF) in the non-coherent, coherent, and proposed hybrid synchronization modes, respectively. The receiver consumes

6.8 mW and 8.8 mW in the non-coherent and coherent mode, respectively, when continuously ON. Using its novel synchronization mechanism, the receiver can reduce the ON time of the receiver by 68% and 34% in order to coherently synchronize and receive a 100-bit and 1024-bit payload, respectively. As a result, the Energy Per Useful Bit (EPUB) of the receiver is reduced by a factor of 2.9 from 1.24 nJ/b to 422 pJ/b for 100-bit payloads, and by a factor of 1.5 from 309 pJ/b to 204 pJ/b for 1024-bit payloads, increasing energy efficiency while maintaining the sensitivity benefits of coherent detection.

Keywords

Ultra-wideband, impulse radio, coherent, non-coherent, synchronization, low power, template-based correlation.

3.1 Introduction

IR-UWB communication is a remarkable solution for low power, low cost, high data rates, and low latency applications such as live data streaming and wearable low power sensor nodes. The IR-UWB receiver detection mechanism generally falls into two main categories: non-coherent and coherent detection.

Non-coherent energy detection has been widely used over the past decade by researchers (Lee, Park, Jang, Jung & Kim (2019); Geng, Liu, Li, Zhuo, Rhee & Wang (2015); Liu, Ni, Zhou, Rhee & Wang (2017)). Its receiver simplicity makes it an efficient approach that can be used in low power/low data rate applications. Non-coherent detection receivers are usually based on energy integration of short UWB impulse signals adhering to UWB spectral emission regulations over a certain time interval, so-called ”integration window”. The presence or absence of the UWB impulse radio (IR) signals determine the amount of integrated energy and therefore ’1’s and ’0’s are typically modulated in simple OOK modulation or pulse-position modulation (PPM) (Lee *et al.* (2019); Geng *et al.* (2015)).

Although the non-coherent receiver offers a reduced receiver complexity, it suffers from lower receiver sensitivity, weak interference rejection capability, and reduced multi-path interference rejection. Several techniques have been proposed to cope with these challenges. A self-interference cancellation technique is proposed in (Lin, Song, Oh, Voroslakos, Kim, Chen, Wentzloff, Buzsaki, Park & Yoon (2022)) to suppress the interference. In (Lee *et al.* (2019)), a digital multi-pulse position modulation scheme (D-MPPM) is proposed to increase the link margin of the transceiver by encoding data with a time difference between the pulses. A synchronized-OOK (S-OOK) modulation scheme is proposed in (Crepaldi *et al.* (2011)) to minimize the synchronization time and reduce the average power consumption of a non-coherent receiver. A spectrum-efficient frequency hopping in (Geng *et al.* (2015)) is proposed to increase the transmission power and enhance the link margin. In (Zhang, Jha, Gharpurey & Kinget (2009)), an analog inter-stage filtering technique is utilized in the receiver to suppress the interferers and spurious image signals.

On the other hand, coherent IR-UWB receivers typically offer better RF performance, increased resilience to blockers and superior inter-symbol-interference (ISI) performance compared to non-coherent receivers. However, their implementation usually comes at the cost of system complexity, due to the need for accurate timing and phase synchronization. This results in increased power consumption. Coherent transceivers can modulate and demodulate phase information in different modulation schemes such as BPSK and QPSK. A two-step discrete-time correlation-based technique for synchronization in the charge domain is proposed in (Liu, Sakurai & Takamiya (2011)) achieving 0.5 ns and 62.5 ps for coarse tuning and fine tuning, respectively. A digitally controlled fine delay correlator is adopted in (Kong, Lee, Kim & Hong (2013)) for synchronizing a MIMO radar array. A phase interpolation (PI) technique for synchronization in a template-based correlation receiver is proposed in (Piraghaj & Saeedi (2019)) in order to increase the time resolution of the trigger of the template signal.

Figure 3.1 shows the common receiver architectures for coherent and non-coherent energy detection IR-UWB receivers. Quadrature analog correlation (QAC) and template correlation are the common implementations in coherent receivers shown in Fig. 3.1 (a) and (b), respectively.

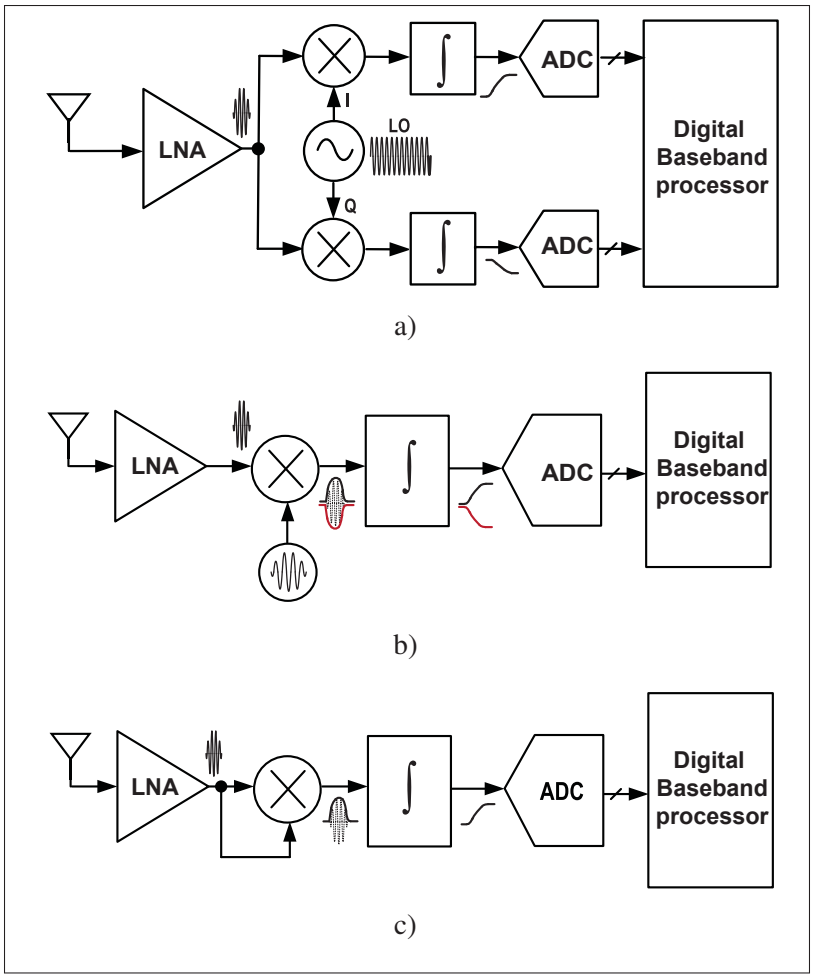

Figure 3.1 Block diagrams of existing IR-UWB receiver architectures: (a) quadrature analog correlation, (b) coherent template correlation, and (c) non-coherent energy detection using self-mixing.

Figure 3.1 (c) shows the energy detection architecture using self-mixing. The QAC architecture usually consumes large amounts of power, since it requires a continuous local oscillator and two distinct signal paths: in-phase (I) and quadrature (Q). The correlation and synchronization in QAC must still take place in the digital baseband processor, and it can be an overhead in the total power consumption of the system (Van Helleputte, Verhelst, Dehaene & Gielen (2009)).

Instead, without necessarily requiring a continuous local oscillator, the template correlation architecture can be implemented with only a single RF signal path by pushing the correlation

into the analog domain. A template signal, ideally the same as the received signal, needs to be generated locally in the receiver and be moved smoothly, until it matches with the received signal. The template generator can be implemented efficiently using a fast startup voltage-controlled oscillator (VCO) and can be duty cycled to minimize its power consumption. A discrete-time digital-IF based on template correlation is presented in (Zhang *et al.* (2009)) requiring high speed ADCs and DACs.

The template correlation architecture seems to be an efficient coherent detection solution. However, the phase synchronization and the initial signal acquisition of the receiver require significant amounts of energy and are challenging to implement. The receiver and the transmitter are blind to each other at the start of a packet sent by a transmitter, and do not have any information about where the IR-UWB signal is within a symbol. This is because the receiver needs to be kept off most of the time to minimize the power consumption. Therefore, a very long preamble is needed before receiving the actual data, so that the receiver can find the received signal and get synchronized to it. This synchronization process has to happen for every packet to remove any clock offset and phase misalignment between the receiver signal and the local template. Consequently, this usually becomes an overhead in the receiver power consumption that can dominate the power consumption profile. This principle has been used in (Miri, Zhou & Heydari (2008)) for high data rates. However, two parallel detection receivers are used and only simulation results are given.

On the other hand, the self-mixing approach shown in Fig. 3.1(c) is a popular non-coherent IR-UWB receiver architecture that does not require any accurate high frequency clock generator (Crepaldi, Angotzi & Berdondini (2019); Liu *et al.* (2017); Lin *et al.* (2022)). This is well-suited to reduced power consumption. Also, the required accuracy of the clock for the non-coherent detection is much less than its coherent counterpart. In non-coherent energy detection receivers, the phase accuracy requirement is relaxed since the signal only needs to fall within the integration window. In other words, the receiver does not necessarily know the exact position of the received signal, and it only attempts to find the best integration window containing the maximum energy of the received signal.

As discussed, symbol alignment between the transmitter and receiver is critically important. The aim of this work is to provide an energy efficient synchronization approach that stems from non-coherent detection in order to reduce the overall power consumption of coherent receivers. This can provide the low-power benefits of non-coherent detection, while allowing for coherent detection's advantages with regards to signal detection.

In the context of IR-UWB low data rate systems, the EPUB is a more realistic metric to compare different architectures and synchronization algorithms than the conventional energy per bit, as it accounts for the preamble overhead as well. In (Crepaldi *et al.* (2011)), a novel synchronized-OOK modulation is proposed where a synchronization pulse always is accompanied by each bit. Although the receiver can achieve agile synchronization, the total EPUB is degraded as synchronization is inevitably happening every bit.

In this work, in order to minimize the EPUB and achieve fast synchronization in a coherent receiver based on template correlation, the initial acquisition of the signal will be achieved non-coherently to a coarse level, and the search scope for the coherent detection is then limited to a single integration window. Afterwards, the coherent fine synchronization, with higher throughput and more timing accuracy, can be performed within the selected integration window. When operating in coherent mode, a template-based coherent architecture is adopted here. Most blocks can be power cycled if the receiver is not actually receiving, hence reducing the average power consumption of the entire system between synchronization and data reception.

The rest of this paper is organized as follows. Section 3.2 introduces the proposed architecture and gives a system description of the receiver. Section 3.3 describes the circuit implementation of the proposed design. Section 3.4 presents the measurement results, and section 3.5 concludes the paper.

3.2 System Description

Timing synchronization is an inevitable task for any IR-UWB transceiver. The main purpose of the synchronization algorithm in non-coherent energy detection receivers is to find the correct

integration window. In coherent energy detection receivers however, accurate phase alignment between the template and the received signal is required. The synchronization becomes more critical and challenging in low power IR-UWB transceivers. In such transceivers, aggressive duty cycling is usually utilized in order to minimize the total power consumption. This is done at certain intervals as depicted in Fig. 3.2 by turning off most of the blocks in the transmitter and the receiver, when no transmission or reception is needed.

Typically, an IR-UWB packet, as shown in Fig. 3.2, consists of three main portions: preamble, syncword, and payload. Each bit in any of the three portions can be '1' or '0' represented by a symbol consisting of a set of pulses. The preamble can be a simple repetitive pattern of consecutive zeros and ones in order for the receiver to synchronize and configure itself to the incoming signal. The preamble has to be long enough for the receiver to have enough time to be synchronized and for the gain to be adjusted through an automatic gain loop to achieve the best performance in the payload section. Before the payload, a syncword, or start of frame delimiter, needs to be transmitted, indicating the starting point of the payload. Importantly, so that the receiver can be successfully synchronized, the preamble duration is correlated to the size of the synchronization search space, which in turn can have an impact on power consumption.

Figure 3.3 shows the conceptual synchronization procedure of a non-coherent receiver (Fig. 3.3(a)), a template-based coherent receiver (Fig. 3.3(b)) and the proposed hybrid synchronization method based on coherent template correlation with non-coherent energy detection assisted synchronization (Fig. 3.3(c)).

In the non-coherent receiver, a symbol time represented as T_s divides into several integration windows of duration T_{INT}. Each pie slice in Fig. 3.3(a) represents an integration window. The total integrated energy within any of these slices that is higher than the others and that exceeds a threshold value will be selected as the correct integration window for demodulation. Since the integrated energy in each slice is done by self-mixing the received signal, there is no need to have any template signal in the receiver. In addition, the minimum required preamble length is minimized, because the search steps are much larger compared to the other two approaches.

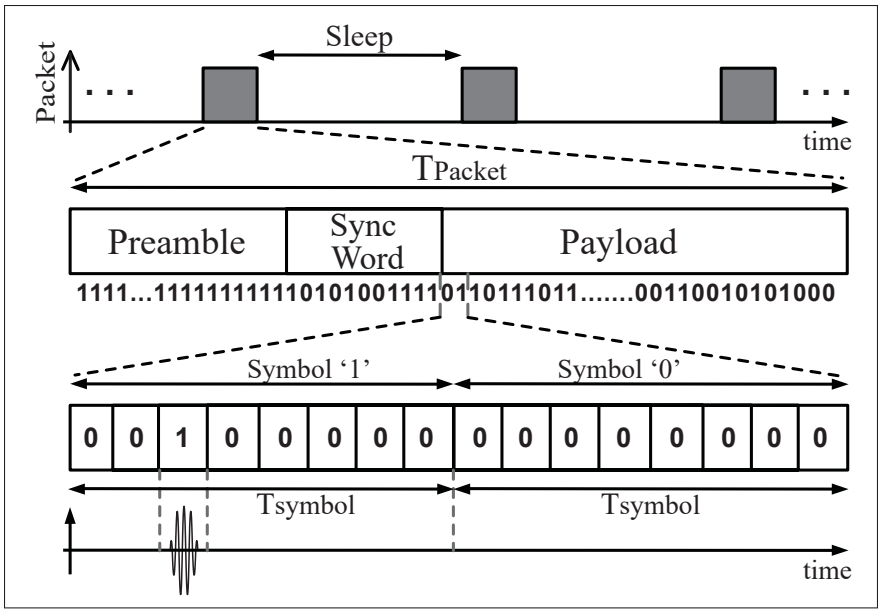

Figure 3.2 IR-UWB packet structure.

As depicted in Fig. 3.3(b), the template-based coherent receiver searches a much larger number of slices of shorter duration Δt (i.e., the minimum time delay resolution) in order to ensure template alignment within a symbol and allow for successful correlation. The correlation happens between the received signal and a known locally generated template signal in the receiver. Since the correlation needs to be done for every Δt, the required preamble length needs to be quite long to provide the time to find the optimal alignment.

Accordingly, the non-coherent receiver can achieve a rapid coarse acquisition without requiring accurate timing synchronization by selecting only the best integration window that contains the most signal energy, while the template-based coherent receiver requires phase synchronization to accomplish the correlation.

As shown in Fig. 3.3(c), in the proposed hybrid method, the coherent search only occurs in an integration window which has been non-coherently selected previously by a non-coherent energy search. An optimal integration window is chosen among all the integration windows after performing a non-coherent synchronization search. Then, the coherent fine acquisition begins within the limited search time of the selected integration window by using a sliding template

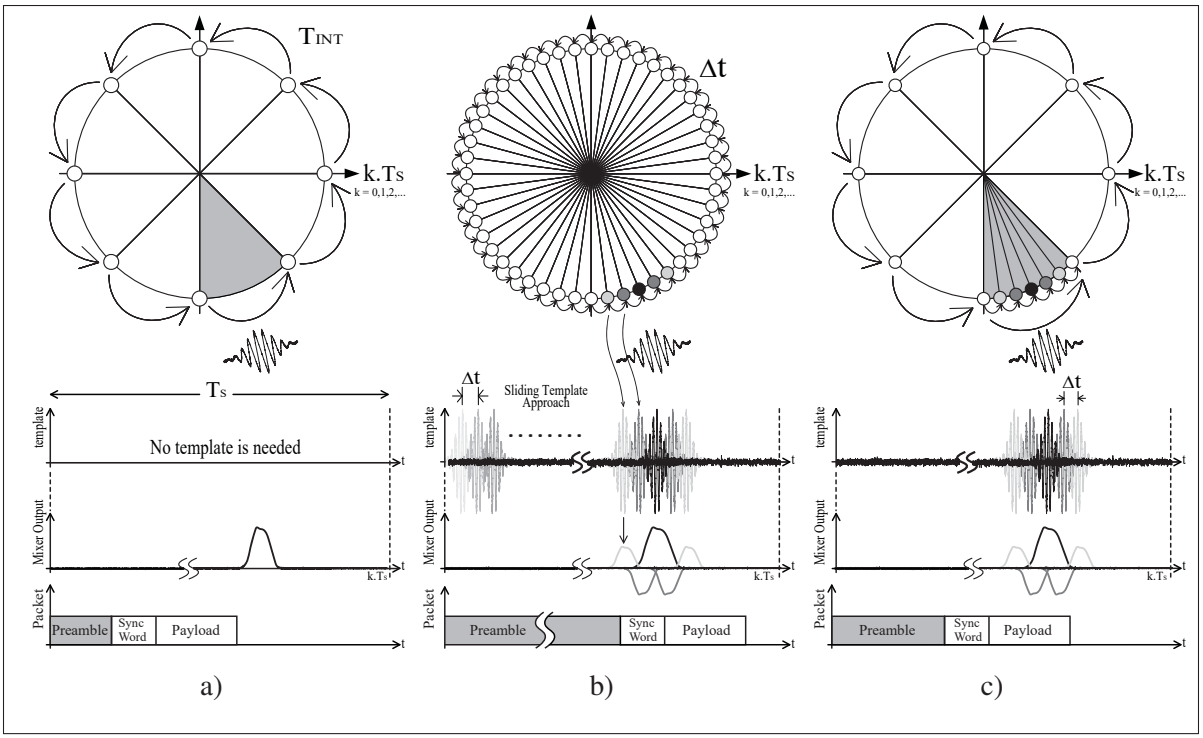

Figure 3.3 Signal diagram of the different energy detection receiver topologies: (a) typical non-coherent self-mixing mechanism, (b) coherent template correlation, and (c) proposed hybrid approach based on coherent template correlation with non-coherent energy detection assisted synchronization.

approach. The template signal moves over the pre-selected integration window in increments of Δt, and the correlator output is evaluated to find the best position of the template to result in the maximum correlation. In this approach, the required time for the coherent synchronization is dramatically decreased because the coherent search is limited to only one integration window (i.e., T_{INT}).

As shown at the bottom of Fig. 3.3, the preamble length is quite dependent on the method used. In the non-coherent mode, the IR-UWB receiver usually requires a short preamble due to the very limited integration window search space. In contrast, coherent mode requires a very lengthy preamble, such that over the duration of the preamble, the receiver searches for a single position

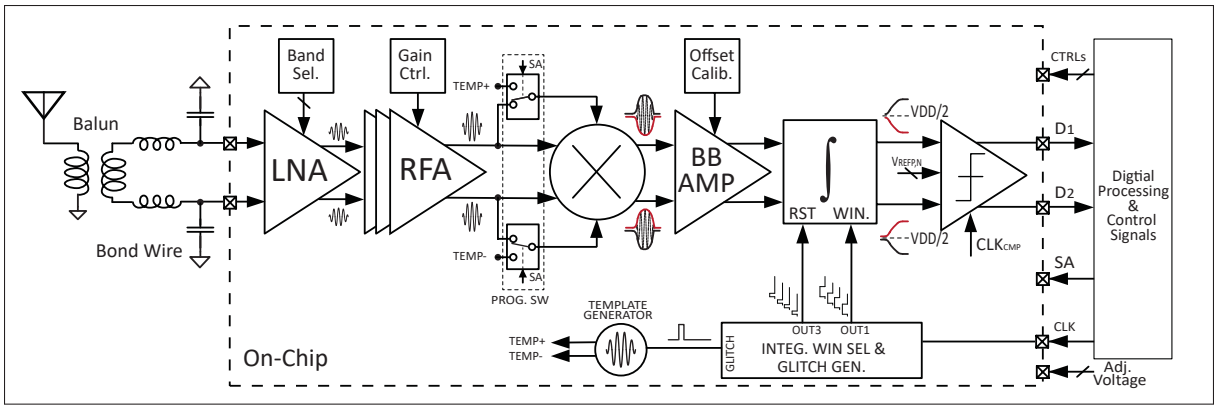

Figure 3.4 Block diagram of the proposed system.

and sweeps the entire symbol time. Due to the hybrid synchronization approach proposed, the required preamble is significantly reduced. As a result, the airtime can be reduced.

The proposed IR-UWB receiver architecture is depicted in Fig. 3.4. It consists of an LNA followed by a variable RF gain stage, a Gilbert-cell mixer, a base-band amplifier with DC offset cancellation circuitry, an integrator, a digitally controlled open loop delay-line, and a comparator. At the heart of the proposed architecture, the mixer is being used as an analog correlator for both the coherent and non-coherent modes. The received signal will be self-mixed and multiplied with a template, in non-coherent and coherent modes, respectively. The output of the mixer will be integrated over a certain period (i.e., the integration window) by the integrator.

3.2.1 Probability of Successful Reception

In coherent receivers, the correlator output is a function of how well the received signal is matched to the template both in frequency and phase. The effect of phase error on the BER of a coherent BPSK receiver in an AWGN channel is given by:

$$P_b(\phi) = Q\left(\sqrt{2E_b/N_0}\,\cos\phi\right), \tag{3.1}$$

where P_b is the bit error probability of the demodulated signal, $Q(x)$ is the Gaussian error function. E_b/N_0 and ϕ are the energy per bit to noise power spectral density ratio and the phase

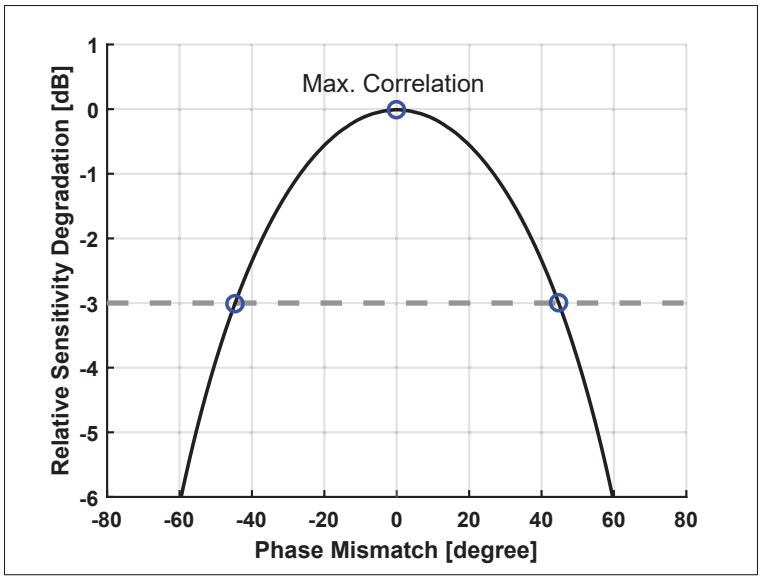

Figure 3.5 Relative sensitivity degradation of the coherent receiver due to phase misalignment.

difference of the local signal and received signal in radians, respectively. According to (3.1), any misalignment in the local carrier or template generator with the incoming signal will degrade the BER performance of the receiver. For instance, a 45 degrees of phase difference leads to a 3 dB loss in E_b/N_0 for a given BER, as shown in Fig. 3.5.

Since the proposed receiver architecture employs different modes and modulation schemes, the minimum required SNR to achieve the same BER value at the baseband processor is different for each of them. As a result, the probability of a random pattern being successfully detected is different in the coherent and the non-coherent modes. The BER performance of a non-coherent receiver operating with OOK modulation and of a coherent receiver operating with BPSK modulation is given by (Arslan, Chen & Di Benedetto (2006); Xiong (2006)):

$$BER_{NC} = Q\left(\sqrt{\frac{\alpha^2 N_S A E_P}{2N_0}}\right), \text{and} \tag{3.2}$$

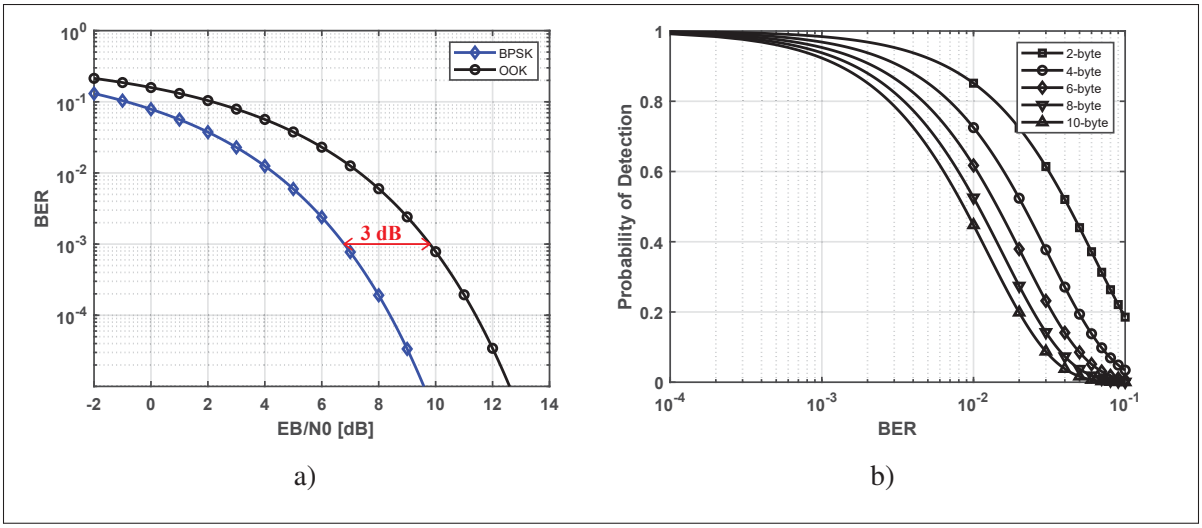

Figure 3.6 (a) BER performances in AWGN channel for non-coherent and coherent receiver based on OOK and BPSK modulation, respectively, and (b) probability of detection for different length random patterns versus BER

$$BER_C = Q\left(\sqrt{\frac{2N_S A E_P}{N_0}}\right), \tag{3.3}$$

where N_S is the number of pulses in a symbol which is equal to 1 in this design, and N_0 is the Power Spectral Density (PSD) of the AWGN at the receiver. The pulse amplitude and energy are represented by A and E_P, respectively. Since a BPSK transmitter sends double the number of pulses than an OOK transmitter for the same random pattern on average, its average output power will not be equivalent. Therefore, α represents the factor that equalizes the average transmitted pulse energy factor in BPSK systems. Figure 3.6 (a) shows the BER performance for the non-coherent and coherent receivers assuming OOK and BPSK modulations, respectively. It is seen that BPSK is 3 dB more efficient than OOK modulation since the Euclidean distances between the constellation points are doubled if the same average power is transmitted in both modulations. ($\alpha = \sqrt{2}$).

For a given E_b/N_0, the probability of a successful reception in non-coherent and coherent receivers is different. The probability of correct detection of N random bits, N_{bit}, can be

estimated as:

$$P_B \simeq (1 - BER)^{N_{bit}}. \tag{3.4}$$

Figure 3.6(b) shows the probability of detection for different random pattern lengths. For instance, a BER of 1.5×10^{-2} is required in order to achieve a 60% probability of correct detection of a 4-byte word. This requires a minimum E_b/N_0 of 3.6 dB in coherent reception. Assuming the same signal to noise ratio for the non-coherent receiver, the probability of correct reception for the same random pattern will be 12%. An estimate of $M = P_{B,C}/P_{B,NC}$ may be used to assess the probability of coherent versus non-coherent reception. For instance, the coherent receiver is $M = 5$ times more likely to correctly detect the 4-byte random syncword pattern than the non-coherent receiver.

For the proposed hybrid method, in order to make the packet in such a way that the coherent and non-coherent portions of the packet have a uniform chance of successful reception, the non-coherent portion of the preamble can be either sent with 3 dB more power, or it can be sent multiple times to equalize the reception chance in the two modes. Sending with 3 dB higher power is a useful approach if the system is not already limited to the peak power limit set by the regulatory. Alternatively, since the chance of detection is M times less in the non-coherent mode than the coherent mode, the non-coherent portion can be repeated M times.

3.2.2 Synchronization

For a non-coherent receiver to be non-coherently synchronized to an incoming signal, the total number of steps is N_{NC}. To find the correct integration window, it is ideally sufficient to perform only one non-coherent search across all of the integration windows, which is the minimum value of N_{NC}. Therefore, only N_{NC} bits for the preamble are needed to allow the receiver to be non-coherently synchronized. For the coherent approach, however, the preamble length must be at least N_C bits, i.e. at least $T_S/\Delta t$, so that the receiver can finely search the entire symbol time frame.

In order for the proposed receiver to get synchronized based on the proposed hybrid approach while having equal probabilities of detection in the non-coherent and coherent detection, the total synchronization steps, N_{NCAC}, can be given using the following equation:

$$N_{NCAC} = M \times N_{NC} + \frac{N_C}{N_{NC}}, \tag{3.5}$$

where N_{NC} and N_C are the required steps for the receiver to be non-coherently and coherently synchronized to the incoming signal, respectively. N_{NC} and N_C can also be written in terms of symbol time as T_S/T_{INT} and $T_S/\Delta t$, where T_S, T_{INT} and Δt are the symbol time, the integration time, and the minimum time delay resolution, respectively. Additionally, M is the factor that equalizes the probabilities of non-coherent and coherent detection.

It should be noted that the required steps for the receiver to adjust its gain and remove DC offset cancellation through the gain control and DC offset calibration loops are not considered in N_{NC} and N_C, and it is assumed that these loops have already been settled. The total energy consumption of the proposed receiver can be estimated as:

$$E_{NCAC} = T_S \cdot \left(N_{NC} \times M \times P_{NC} + \frac{N_C}{N_{NC}} \times P_C \right), \tag{3.6}$$

where P_{NC}, P_C, and P_{NCAC} are the receiver's average power consumption in non-coherent, coherent, and the proposed hybrid approach, respectively. Since N_C and P_C are usually larger than P_{NC} and N_{NC}, the average energy consumption of the proposed approach would be dominated by the coherent mode.

It can be also observed that the energy consumed for the coherent reception in the proposed hybrid synchronization approach can be reduced by a factor of $K \simeq N_{NC}$ when compared to the template-based coherent receiver approach. Even though the energy consumption of the non-coherent portion has increased, the reduction of energy consumption in the coherent portion is more significant than the increase in energy consumption in the non-coherent portion. Furthermore, the energy per useful bit in the receiver can be estimated as (Ammer & Rabaey

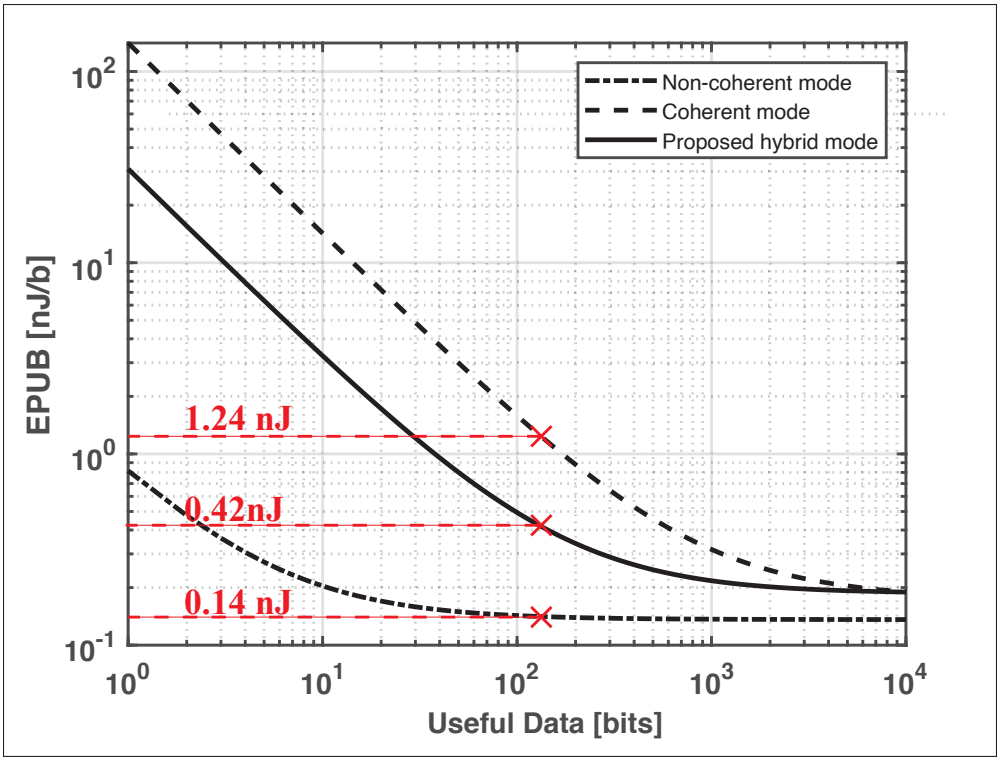

Figure 3.7 Simulated EPUB comparison of different detection modes at a PRF of 50 MHz.

(2006)):

$$EPUB_{RX} = \frac{B_{Preamble} + B_{Data}}{B_{Data}} \cdot P_{RX} \cdot N_S \cdot T_S, \tag{3.7}$$

where $B_{Preamble}$ is the number of bits in the preamble and B_{Data} is the total number of bits in the syncword and payload. P_{RX} and N_S are the average power consumption of the receiver without any duty-cycling and the number of impulses in each symbol, respectively. The preamble overhead, $(B_{Preamble} + B_{Data})/B_{Data}$, degrades the EPUB as no useful information is transferred during synchronization. Reducing the preamble length results in a reduced preamble overhead and a reduction in synchronization time if the receiver is able of synchronising sufficiently fast. (Ryckaert, Verhelst, Badaroglu, D'Amico, De Heyn, Desset, Nuzzo, Van Poucke, Wambacq, Baschirotto & others (2007)).

Considering the power consumption reduction factor, K, of the proposed hybrid synchronization method that stems from having $N_{INTEG_{WIN}}$ smaller integration windows within a symbol,

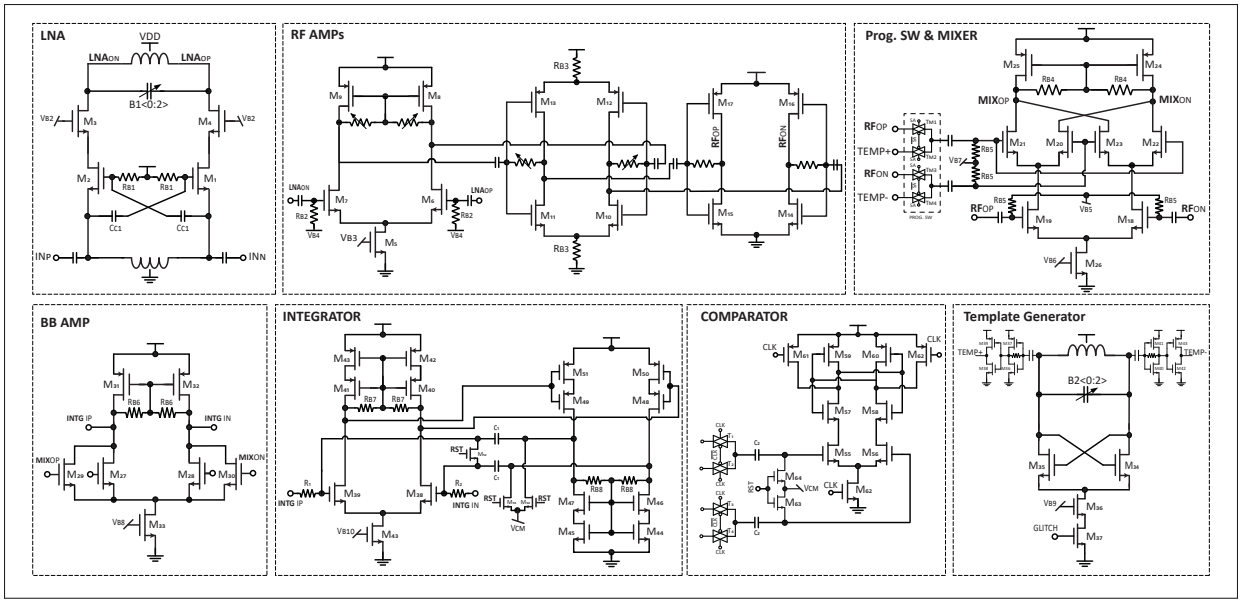

Figure 3.8 Transistor-level implementation of the proposed receiver with labelled sub-blocks.

and the ratio, M, between the probabilities of successful reception for coherent detection and non-coherent detection of a 4-byte random pattern which was seen to be 5 for a 60% reception probability, it can be said that the minimum value for $N_{INTEG_{WIN}}$ is M.

In this design, the PRF is 50 MHz and $N_{INTEG_{WIN}}$, i.e. the total number of integration windows, is equal to 5 to accommodate a uniform coherent/non-coherent detection probability for a 4-byte word. According to the relative sensitivity result as is shown in Fig. 3.5, the receiver will be within a -1 dB performance degradation if the phase misalignment is less than ~25 ps.

As a result, the total steps for the synchronization in the non-coherent mode is N_{NC} = 5, as there are 5 integration windows in a symbol, and in the coherent mode N_C = 800. Altogether, these steps will be reduced to N_{NCAC} = 185 for the proposed approach.

Fig. 3.7 illustrates the EPUB comparison of the non-coherent, coherent, and proposed hybrid mode at 50 MHz pulse repetition frequency (PRF), assuming there are 5 integration windows in the receiver. It can be seen that non-coherent energy detection can achieve the lowest EPUB for any packet size. The highest number of EPUB always results from a coherent template

correlation. The proposed hybrid synchronization, as previously discussed, can approximately reduce the packet size by a factor $K \simeq N_{NC}$. Consequently, the EPUB value is reduced from 1.24 nJ/b to 0.42 nJ/b for 132 useful bits, including a 32-bit syncword and a 100-bit payload, and from 0.3 nJ/b to 0.2 nJ/b for 1024-bit payload. Overall, our proposed hybrid method allows to reduce the time required to coherently synchronize to the input signal, and thus reduces the energy footprint of the coherent synchronization. Overall, this hybrid method allows to reduce the time required to coherently synchronize to the input signal, and thus reduces the energy footprint of the coherent synchronization.

3.3 Circuit Implementation

The receiver is designed to operate in the 3.5, 4, 4.5, and 5 GHz bands in order to support the 802.15.4a IEEE standard (Group & others (2003)). The circuit implementation for each of the blocks composing the proposed receiver is shown in Fig. 3.8. Each block is detailed below.

3.3.1 LNA and RF Amplifier

A cross-coupled differential common gate low noise amplifier is designed to operate from 3 to 6 GHz. The common gate LNA is selected over the other LNA topologies due to its wideband input matching (Zhuo, Li, Shekhar, Embabi, de Gyvez, Allstot & Sanchez-Sinencio (2005); Liao & Liu (2007)) in order to support the UWB signal, which has a minimum 500 MHz bandwidth. The wideband LNA can be achieved through a low Q-factor source inductor. Moreover, G_m-boosting using capacitive cross-coupling improves the NF performance of the LNA without a power consumption penalty (Zhuo *et al.* (2005)). The cascode transistors further help to lower the input impedance of the LNA.A 2-bit capacitor bank at the output of the LNA can tune the center frequency to achieve a reconfigurable frequency band, which can be used for multi-user concurrent applications.

Typically, one stage of signal amplification is not sufficient to achieve a reasonable link budget. Here, three variable RF gain amplifiers are also cascaded to boost the RF gain and suppress the

noise of the following stages. Note that, since the signal is already being amplified by the LNA, the NF requirement of these RF stages is not as strict as that of the LNA. The gain control of the RF amplifier is achieved in an analog fashion and is controlled off-chip. The gain is adjusted if the SNR at the receiver is too high to avoid saturating the next stages and desensitizing the receiver. The total gain can be varied by 30 dB, using an analog voltage from 0 to 1 V.

The first stage of the RF amplifier is a differential RF amplifier with active loads, as shown in Fig. 3.8. This architecture also improves the common mode rejection ratio of the receiver. Two proceeding cascaded amplifiers are common source current-reuse amplifiers where the common mode rejection ratio is further suppressed at the second stage by using 100-ohm degeneration resistors on both tails. These two resistors are implemented using transistors operating in the triode region. As the signal being amplified along the chain gets larger, the linearity and signal swing range become more important. As such, the last stage is a high swing amplifier without any gain reconfigurability or source degeneration resistors, as it they limit the maximum output swing of the amplifier.

3.3.1.1 Mixer, BB amplifier and Programmable Switch

A conventional Gilbert-cell mixer is utilized in order to achieve high conversion gain and improve receiver sensitivity. One of the differential inputs of the mixer is connected to the output of the RF amplifier, while the other input can be either connected to the template generator to make coherent detection possible, or to the RF amplifier to make a self-mixer and enable non-coherent detection. The output of the mixer which has a 500 MHz bandwidth is fed to the integrator, and the energy of the signal is measured over the integration window. Since the signal is already amplified in the LNA and RF amplifier stages, a simple low loss analog multiplexer based on transmission gates is used to switch the mixer input with good linearity.

3.3.1.2 Integrator and Comparator

An active-RC integrator is a good candidate for low/moderate frequency operation, while providing high dynamic range. Further, it can be highly linear as very linear resistors and capacitors can be used. A fully differential comparator compares the integrated energy at the output of the mixer with the differential threshold voltages, controlled off-chip.

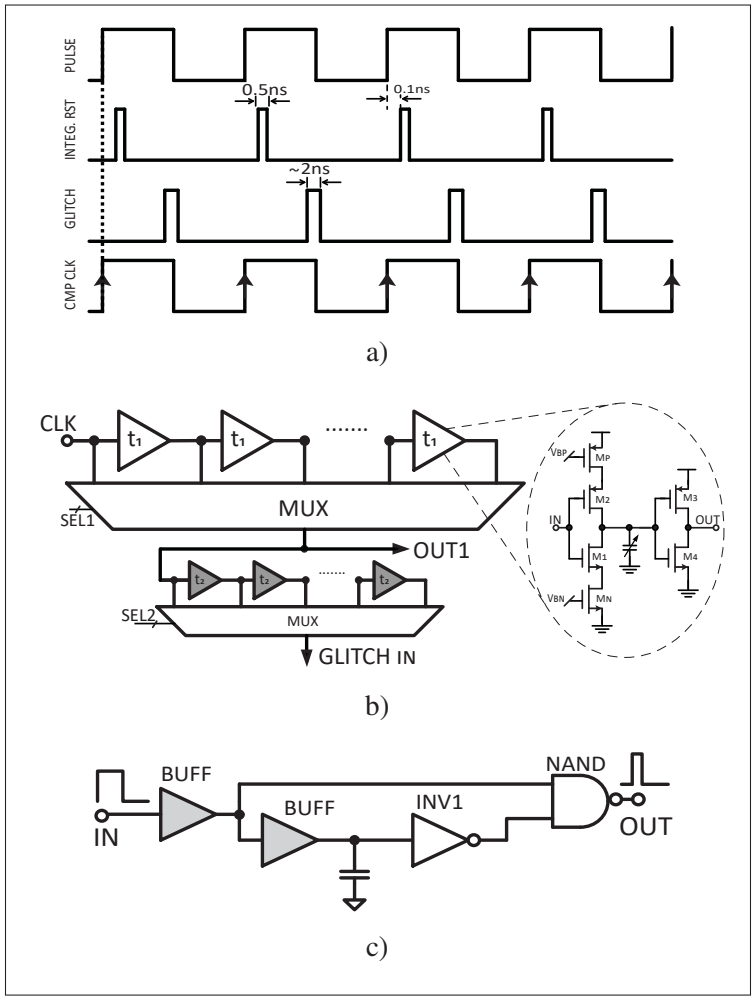

Figure 3.9 (a) Timing diagram of the different blocks of the proposed receiver, (b) two-step delay line, and (c) glitch generator.

The timing diagram for the operation of the integrator comparator is depicted in Fig. 3.9(a). The reset signal of the integrator (INTEG.RST)is a glitch generated from the rising edge of the

symbol clock (PULSE). This narrow glitch resets the integrator output to $V_{DD}/2$. It is designed in such a way that there is 0.1 ns delay after a rising edge and it has a 0.5 ns duration. Before the integrator gets reset, the comparator also must have time to regenerate its outputs at the rising edge of its clock (CMP CLK). The comparator will be in reset phase when CMP CLK is low. During the reset phase, the top plate of the comparator's input capacitor will be reset to V_{CM}, which is equal to $V_{DD}/2$. Transmission gates T1 and T3 connect the integrator's two outputs to the bottom plate of the capacitor, while the integrator is in the reset phase. Hence, the capacitors will be charged during the first phase to $V_{CM}\check{}V_{IN}$. Afterwards, V_{CM} is disconnected from the capacitors and only T2 and T4 will connect the differential voltages to the bottom plate of the capacitors. Thus, the voltage at the input of the comparator pair, i.e., M55 and M56 transistors at the rising edge of the CMP CLK signal, will be $V_{CM}\check{}V_{IN}\check{}V_{REF}$.

3.3.1.3 Delay-locked loop and Template Generator

To achieve coarse and fine synchronization, a two-step open loop DLL has been utilized. Longer delay cells are used to generate the coarse delays, while shorter delay cells provide the fine delay tuning for the pre-selected coarse phase. Each of the selected phases can be finely tuned to achieve fine synchronization. The coarse delay phases are mainly used for the best integration window to be selected during the non-coherent coarse synchronization. This is done so in order to determine the best phase, resulting in the maximum integrated energy of the received signal. At the same time, the fine delay tuning adjusts the trigger signal of the template generator, in order to be able to slide it over the pre-selected coarse phase in a template-based coherent synchronization approach, as illustrated in Fig. 3.3(c). Since the position of the received signal is random and can be on the integration edge, the delay line is designed such that each of the coarse delay elements has less delay, approximately 175 ps, than the total delay of the fine delay cells. In other words, $t_1 \leq m \cdot t_2$, where m is the total number of fine delay cells, t_1 is the coarse delay cell delay and t_2 is the fine delay cell delay. As a result, the DLL line has some overlapping delays, and the total delay of the two-stage delay line is not strictly increasing when the digital

control codes are going from 0 to the last code. These overlapping delays avoid non-optimal correlation results when the received signal is on the edge of the integration window.

To enable the coarse and fine timing required by the proposed hybrid method, a two-step open loop DLL is used. Figure 3.9(b) shows the block diagram of the two-step DLL. The upper delay cells (t_1) are 2^5 cells based on a current starved delay element, while the lower fine-tuning delay cells (t_2) are 2^5 cells based on minimum size buffers with low threshold voltage transistors in order to achieve the required fine 25 ps delay for each cell. The capacitor bank at the output of the first current starved stage, as well as its bias current, can tune the propagation delay of the delay cell. The coarse tuning delay cells are designed to provide a 625 ps delay. An overlap delay that is equal to seven fine codes is considered in the DLL, in case the received signal is on the edge and avoids non-optimal correlation in the coherent mode.

The template generator is implemented by using a fast start-up LC voltage controlled oscillator (VCO) designed to operate in the receiver's band of operation. A glitch generator as is shown in Fig. 3.9(c) is designed to generate narrow pulses, in the order of 2 ns duration glitches (GLITCH in Fig. 3.9(a)). These narrow glitches which can be coarsely and finely tuned by the DLL toggle ON and OFF the fast start-up VCO for a short amount of time. As a result, a gated template UWB signal is generated at the output of the VCO. Additionally, the VCO can be coarsely and finely tuned to oscillate at the same center frequency of the receiver front-end using a 2-bit capacitor bank and a CMOS varactor, respectively.

3.4 Measurement results

The proposed IR-UWB receiver was designed and implemented in 65 nm CMOS technology. The chip micrograph and the designed PCB are shown in Fig. 3.10. The total active die area including pads is 1.24 mm^2. A good correlation between the DC power consumption of the receiver in simulation and measurements is measured. The receiver consumes 6.8 mA and 8.8 mA from a 1 V supply when continuously ON, excluding the buffers and the digital baseband processor, in non-coherent mode and coherent mode, respectively. The receiver is duty cycled

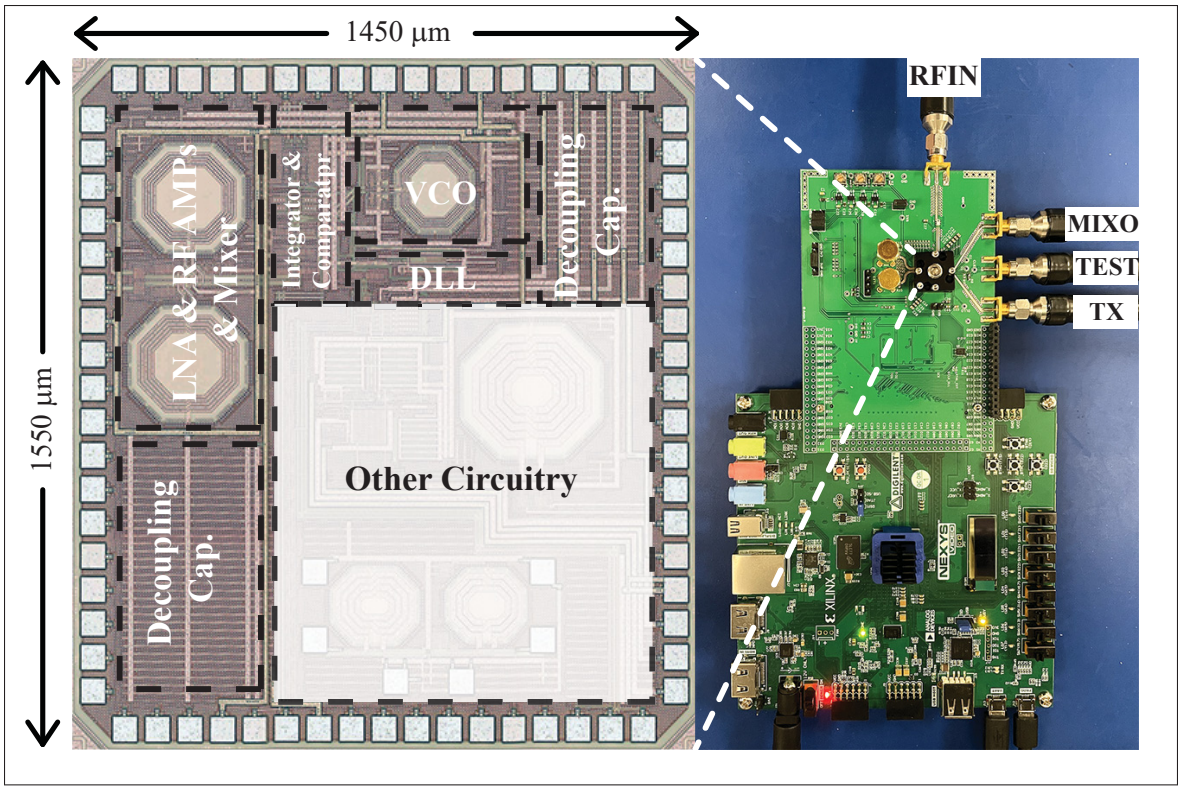

Figure 3.10 Micrograph of the proposed receiver and the designed test PCB.

at a 1 kHz packet rate to reduce its power consumption in all measurements. This resulted in 19 μW(145 μW), 164 μW(325 μW), and 52 μW(215 μW) average power consumption with duty-cycling of 0.28% (2.1%), 1.9% (3.7%), and 0.6% (2.4%) for a packet with a 100-bit payload (1024-bit payload) in the non-coherent mode, coherent mode, and the proposed hybrid synchronization mode, respectively.

The time-domain results including the entire transmitted packet, and a zoomed view at the end of the preamble reception are shown in Fig. 3.11 for the three different modes: (a) non-coherent detection, (b) coherent detection, and (c) the proposed hybrid method. The preamble in all of the different modes is a successive OOK modulated "1" symbol. While the 32-bit syncword (‘0xE620A5DB’) and payload are OOK modulated signals for non-coherent detection and BPSK modulated signals for template correlation. The received signal at the input of the receiver and the output of the mixer can be seen in each plot in blue and red, respectively. As can be seen, the

output of the mixer in non-coherent mode always results in a positive signal that corresponds to a ‘1’, while the absence of the positive signal corresponds to a ’0’. On the other hand, since the phase is also encoded in the coherent mode and the proposed method, positive and negative signals can be seen at the output of the mixer.

Moreover, the $PREAMBLE$ and $D_1 - D_2$ signals are labeled in Fig. 3.11 where the former shows when the receiver is synchronized during the preamble reception and the latter is the digital differential output of the receiver. As can be seen, in the non-coherent mode, $D_1 - D_2$ toggles between ’0’ and ’1’, while in the coherent mode and the proposed method it toggle between ’-1’ and ’1’ during the packet reception. In that case, the ’-1’ is decoded as a ’0’ in the figure.

Furthermore, the required packet length with the same 4-byte syncword and 1024-bits payload takes about 21.22 μs and 37.12 μs in the non-coherent and coherent modes, respectively. The preamble size is only 5 bits in the non-coherent mode, whereas, it is 800 bits in the coherent mode. In this case, the coherent receiver can get synchronized and find the best phase after 480 bits of the preamble.

Alternatively, in the proposed hybrid synchronization method, the packet length for a 1024-bit payload is reduced to 24.42 μs by doing a non-coherent search at the beginning of the preamble. This resulted in a 34.2 % reduction in the required packet length for a successful coherent detection, from 37.12 μs in the template correlation detection to 24.42 μs in the proposed hybrid method, while requiring only a 3.2 μs increase in the air time compared with the non-coherent detection. Using a 100-bit and 2048-bit payload, the required packet length was reduced by 68 % and 22 % by the proposed hybrid method, respectively. This shorter packet in the proposed hybrid synchronization method allows for lower duty operation for the receiver, allowing for lower power consumption, while still yielding the advantages of coherent detection within the payload.

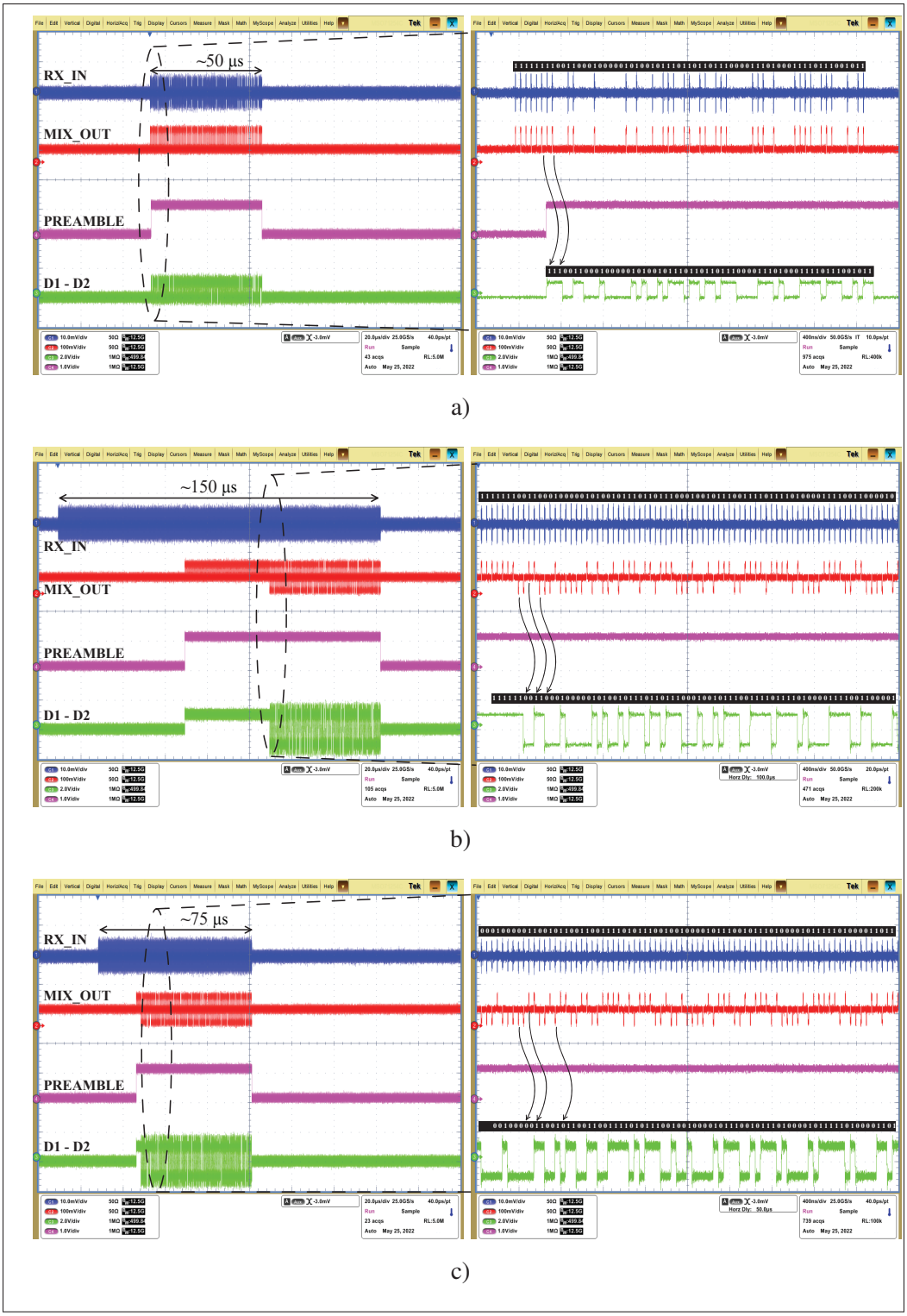

Figure 3.11 Measured time domain waveform in (a) non-coherent detection, (b) coherent template detection, and (c) the proposed coherent template correlation with non-coherent energy detection assisted synchronization.

The receiver front-end can operate at 4 different bands, spaced by 500 MHz, at 3.5, 4, 4.5, and 5 GHz. Figure 3.12 shows the normalized power in different bands at the output of the mixer. It can be seen that the receiver can achieve 5 dB band-to-band isolation.

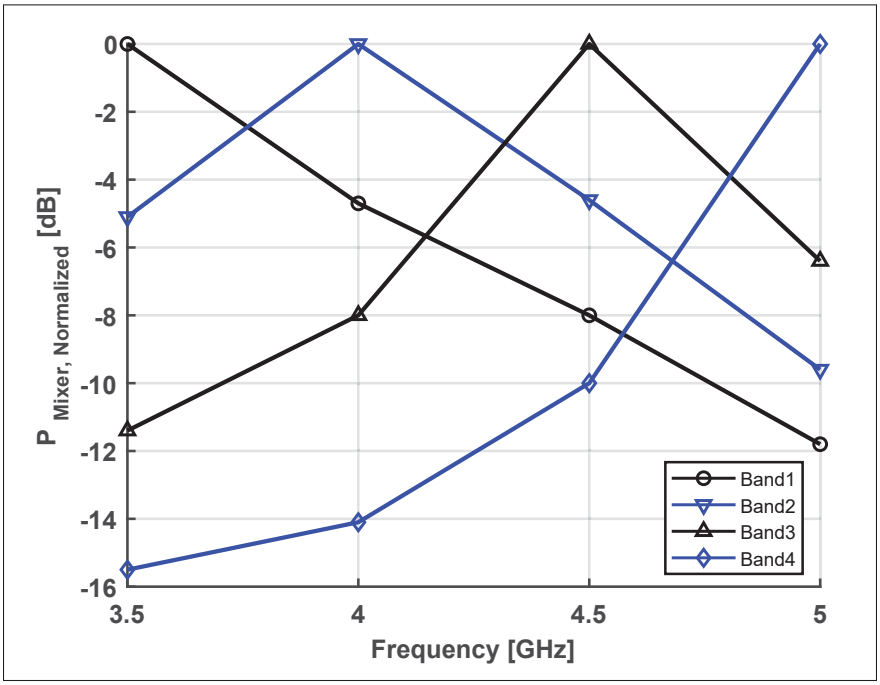

Figure 3.12 Normalized received power at the mixer output in different bands of the receiver.

The BER results of the receiver in the non-coherent, coherent modes and proposed hybrid mode are shown in Fig. 3.13. For the BER measurement, the attenuation is swept with a variable attenuator (Agilent J7211C) in a cabled link. An arbitrary waveform generator (Tektronix AWG7122C) generates the input RF signal. For each attenuation value, 500 pseudo-random packets containing 2048 bits each, at a 1 kHz packet rate, are sent. The measured receiver sensitivity in non-coherent mode, coherent mode and the proposed hybrid mode are -68 dBm, -70.5 dBm and -70.8 dBm at a 50 MHz PRF for a 10^{-3} BER, respectively. It is noted that the average input power is measured by sending consecutive ones and the received power at the receiver input is integrated over the receiver bandwidth. The spectrum analyzer (Agilent PXA N9030A) was configured to 1 MHz and 3 MHz of RBW and VBW, respectively. As can be seen from Fig. 3.13 the coherent reception outperforms the non-coherent mode by 2.5 dB at

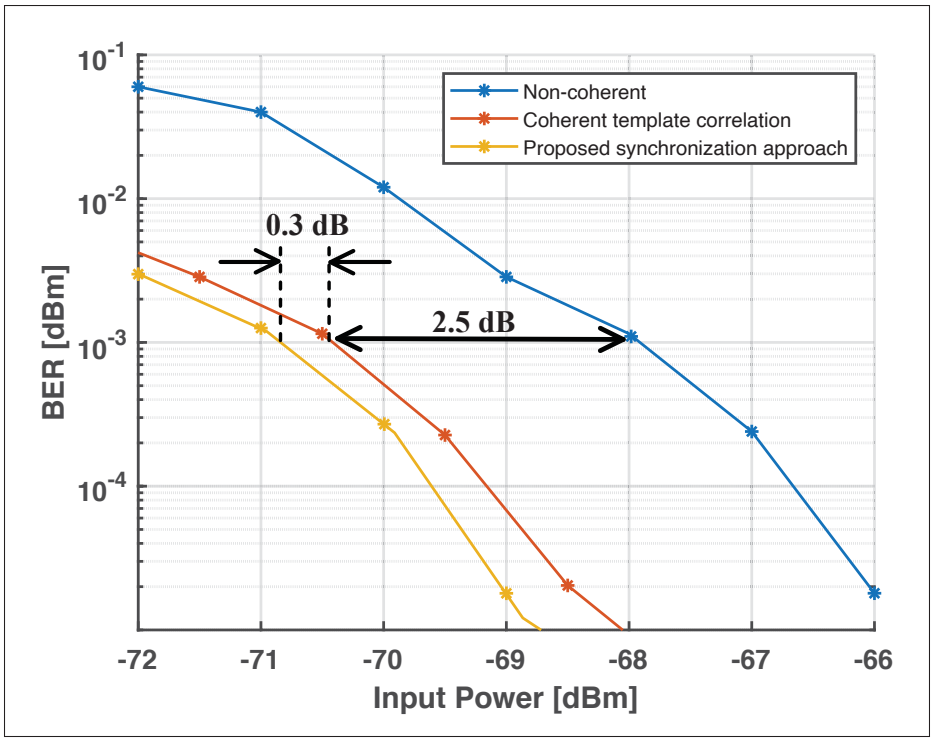

Figure 3.13 BER result comparison of the non-coherent and coherent fully coherent template correlation mode and proposed coherent template correlation with non-coherent energy detection assisted synchronization.

10^{-3} BER in measurements, which agrees well with the 3 dB theoretical advantage of BPSK vs OOK. The proposed coherent template correlation with non-coherent energy detection assisted synchronization method achieves 0.3 dB extra receiver sensitivity improvement compared to the fully coherent receiver, mainly due to the packet length reduction which can reduce the impact of the DLL jitter for the last bits in the payload.

As the bandwidth of the receiver is wide, it is likely that a blocker can desensitize the receiver given the fact that the total front-end gain is relatively high in order to achieve acceptable receiver sensitivity performance. Moreover, out-of-band transmissions raise the noise floor in the UWB band and worsen the sensitivity of the UWB receiver. Therefore, interference suppression is critical for such receiver.

To assess the interference robustness, the receiver performance has been evaluated in the presence of two interferers. The receiver is configured to operate at 50 MHz PRF in the 4 GHz band. Two WiFi signals at 2.4 GHz and 5.1 GHz with 802.11a modulation and 20 MHz of bandwidth are added to the original UWB AWG signal. The UWB signal is set to be 3 dB above the receiver sensitivity, i.e. at -65 dBm and -67.5 dBm for the non-coherent mode and coherent mode, respectively. It is noted that the power of the UWB signal is also backed-off by 3 dB for the coherent mode in order to receive the same power at the receiver input. This is due to the BPSK modulation which doubles the number of UWB impulses in comparison to OOK modulation. The measured BER drops to 10^{-3} BER when the integrated out-of-band interference power is -24.5 dBm and -16.5 dBm for non-coherent detection and coherent detection, respectively. This translates to a -49 dB and -54.5 dB out-of-band signal-to-interference Ratio (SIR) for non-coherent mode and coherent mode when the received power is 3 dB above the receiver sensitivity, respectively. The coherent mode thus outperforms the non-coherent mode by 5.5 dB in terms of out-of-band SIR.

The measurement results are summarized and compared with previously published designs in Table 3.1. Thanks to the reconfigurability in the proposed receiver‘s architecture and the multi-resolution DLL, both coherent and non-coherent detection can be supported without requiring an additional receiver front end. Whereas, other state-of-the-art receiver architectures mainly support solely a single modulation.

As opposed to the complex receiver architecture used in (Kim & Rabaey (2016)), a coherent receiver is implemented here with a simplified receiver architecture and lower power consumption that can be used for low power and low data rate applications. A higher PRF can result in lower EPUB numbers as reported in (Kim & Rabaey (2016); Lee *et al.* (2019)). It is anticipated that the EPUB generated in (Kim & Rabaey (2016); Lee *et al.* (2019)) will be significantly degraded if the data rate is reduced. Due to duty cycling of the receiver in the proposed work, it is able to consume low amounts of power while maintaining the same data rate, as compared to (Vigraham & Kinget (2014)).

Table 3.1 PERFORMANCE SUMMARY AND COMPARISON WITH PREVIOUS IR-UWB RECEIVERS

	Year	Tech. (nm)	Supply (V)	Data Rate (Mbps)	Freq. (GHz)	Area (mm2)	Modulation	Approach	Power (mW)	Sen. (dBm)	Energy per bit (pJ/b)	EPUB (pJ/b)
Lee *et al.* (2019) JSSC' 19	2019	65	1.1	500	3-5	2.88	D-MPPM	time difference detection	27.7	-61	69	N/A
Liu *et al.* (2017) JSSC' 17	2017	180	1.8	1	3.0-4	5.6	OOK	asynchronous ED	0.42	-74	420	N/A
Song, Liu, Zhang, Rhee & Wang (2019) JSSC' 19	2019	65	1	5	6.5-8.1	2.66	PPM	non-coherent ED	6	-69	1200	N/A
Kim & Rabaey (2016) JSSC' 16	2016	65	1	1000	3.1-10.6	4.6	BPSK	coherent QAC	20.9	-74	102	102
Vigraham & Kinget (2014) JSSC' 14	2014	65	1	2	4.35	0.53	OOK	non-coherent time slicing	0.75	-76.5	375	395
Crepaldi *et al.* (2011) JSSC' 11	2011	90	1	1	3.6-4.3	2.2	S-OOK	non-coherent ED	2.18	-66	2180	2180
This work	**2022**	**65**	**1**	**1 / 2** †	**3.5-5**	**1.24**	**OOK**	**non-coherent ED**	**0.019 / 0.145**†	**-68**	**136**	**141 / 136**⋆
							BPSK	**coherent ED**	**0.164 / 0.325**†	**-70.5**	**176**	**1240 / 309**⋆
							OOK/BPSK	**hybrid synchronization ED**	**0.052 / 0.215**†	**-70.8**	**176**	**396 / 204**⋆

ED = Energy Detection. QAC = Quadrature Analog Correlation
All measurements are done with proper duty cycling of the receiver at 1 kHz packet rate.
† Measured for a packet with a 100-bit payload (first value) and a 1024-bit payload (second value). The power consumption of the digital baseband processor and the off-chip CLK generation are not included.
⋆ EPUB numbers are measured for a packet consisting of a 100-bit payload (first value) and a 1024-bit payload (second value) with 5-bit, 800-bit, and 185-bit preamble in non-coherent ED, coherent ED, and hybrid synchronization modes, respectively.

As a result of the proposed synchronization approach, the receiver's ON time and preamble overhead are reduced. The proposed hybrid synchronization method helps to reduce the EPUB by a factor of 2.9 from 1.24 nJ/b for the coherent mode based on BPSK modulation to 422 pJ/b in a packet with a 100-bit payload by reducing the packet length from 18.6 μs to 5.9 μs. For a long packet with a 1024-bit payload, the proposed synchronization method can reduce the EPUB by a factor of 1.5 from 309 pJ/b for the coherent mode to 204 pJ/b. The proposed approach can thus compare favorably to the non-coherent receivers reported in (Vigraham & Kinget (2014)) and (Crepaldi *et al.* (2011)) in terms of EPUB. Even though the latter is based on synchronized-OOK modulation where the non-coherent synchronization time is 0, the EPUB is significantly high. This is because the synchronization is inevitably happening every bit, rather than every packet as proposed here. As a result, that receiver needs to remain fully ON, thus degrading the EPUB. In addition to improving the energy efficiency of the receiver, the proposed method allows for shorter packets than that of coherent detection while providing similar payload decoding

sensitivity. These shorter packets can allow for reduced latency communication without having to resort to fully non-coherent detection, and reduced sensitivity.

3.5 Conclusion

This paper describes a low power, coherent IR-UWB receiver that uses non-coherent assisted synchronization and is implemented in 65 nm CMOS technology. The proposed receiver architecture enables demodulation of OOK and BPSK in non-coherent and coherent modes, respectively. Additionally, it offers a hybrid synchronization method for efficient reception and fast synchronization.

The proposed hybrid synchronization method realizes an initial non-coherent search in order to limit the search space for coherent synchronization and reception in a sliding template correlation receiver. As a result, the required preamble length is reduced below what is required by coherent preamble detection, allowing for reduced power consumption while maintaining the sensitivity benefits of coherent payload detection.

The receiver consumes 6.8 mW and 8.8 mW when operating fully ON in non-coherent and coherent modes, respectively. A multi-resolution DLL and fast start-up VCO are used to provide the proper phase for the integration window as well as the template generation, respectively. The receiver operates from 3.5 to 5 GHz over four bands, each spaced by 500 MHz, and achieves a -68 dBm, -70.5 dBm, and -70.8 dBm sensitivity at a 10^{-3} BER at 50 MHz PRF in the non-coherent, coherent, and the proposed hybrid mode, respectively. The receiver architecture is robust to modulated narrow-band interference levels of up to -24.5 dBm and -16.5 dBm in the non-coherent and coherent modes, respectively.

Accordingly, this work paves the way for low power operation of IR-UWB receivers that can nonetheless benefit from coherent payload detection. The synchronization method proposed in this work thus allows receivers to drastically reduce synchronization energy overhead by 2.9 times and air time by 68% for a 100-bit payload packet reception over that of coherent detection.The significantly reduced synchronization time improves the receiver EPUB and,

potentially, that of a matching transmitter. It is thus well-suited to low power applications by reducing the packet transmission and reception times, enabling lower duty cycles.

3.6 Acknowledgement

The authors would like to thank the Natural Sciences and Engineering Research Council of Canada (NSERC) for their financial support, and CMC Microsystems for providing the CAD tools and CMOS technology access.

CONCLUSION AND RECOMMENDATIONS

The main goal of this thesis was to exploit a low-power efficient coherent IR-UWB receiver. Coherent reception can provide better RF performance and is more robust to interference and blockers compared to non-coherent receivers. However, the higher receiver's complexity and power consumption have made non-coherent receivers more welcome in low-power applications due to their ease of implementation.

The main contribution of this thesis was the design and fabrication of a coherent IR-UWB receiver with non-coherent assisted synchronization, which allows for the realization of an energy-efficient solution for coherent receivers by reducing the energy footprint of the frame synchronization.

In the proposed synchronization algorithm, a non-coherent energy detection starts to find the integration window among all of the potential windows that best fits the signal energy to achieve coarse-level synchronization. This gives a rough estimation of the delay of the incoming signal and allows the receiver to reduce the aggregate noise. Then, a coherent synchronization comes into play and searches accurately within the pre-selected integration window to allow for fine synchronization over a reduced search space, allow for a reduced energy requirement for synchronization and for subsequent coherent demodulation of the payload.

A prototype of the proposed receiver front-end, including the LNA, mixer, baseband circuitry, VCO, and DLL were implemented in 65-nm CMOS technology. As was presented in chapter 3, the proposed receiver architecture achieves a -68 dBm, -70.5 dBm, and -70.8 dBm sensitivity at a 10^{-3} BER at 50 MHz PRF in the non-coherent, coherent, and proposed hybrid synchronization modes, respectively. The receiver consumes 6.8 mW and 8.8 mW in the non-coherent and coherent mode, respectively, when continuously ON. Using its novel synchronization mechanism, the receiver can reduce the ON time of the receiver by 68% and 34% in order to coherently synchronize and receive a 100-bit and 1024-bit payload, respectively. As a result, the EPUB of

the receiver is reduced by a factor of 3.1 from 1.24 nJ/b to 396 pJ/b for 100-bit payloads, and by a factor of 1.5 from 309 pJ/b to 204 pJ/b for 1024-bit payloads, increasing energy efficiency while maintaining the sensitivity benefits of coherent detection.

Future Work

To continue the work started during this master's, several recommendations can be made. The recommendations can be summarized as follow:

The performance of the designed receiver has to be evaluated over the air in both coherent and non-coherent modes, as well as the proposed synchronization algorithm.

In order to perform any over-the-air tests, an antenna needs to be designed for the receiver and the transmitter. The design of wideband different antenna types, such as a monopole and Vivaldi antennas needs careful consideration.

An AWG is used instead of a transmitter in this thesis. The design and implementation of an IR-UWB transmitter that supports both OOK and BPSK modulations will enable a complete transceiver to be implemented.

The receiver has the potential to be improved to obtain a better NF. It seems that the RF gain in the receiver chain needs to be increased. This can be done by adding another RF amplifier stage. It will improve the receiver sensitivity of the receiver by a few more dBs.

The off-chip transmission line as well as the mutual coupling of the on-chip inductors could be carefully designed using 3D electromagnetic simulation software such as Ansys HFSS and ADS. While no significant impact was identified during experimental tests, this may allow for improved RF performance.

Finally, it is suggested that the next iteration of the receiver goes to the higher band of the UWB band, i.e. 6 GHz to 9 GHz, as it is supported more universally worldwide by regulatory bodies such as ETSI in Europe. For this prototype, since the main goal was to demonstrate and evaluate the architecture and the synchronization method, the lower band from 3.1 GHz to 6 GHz was selected for the sake of a more straightforward design.

APPENDIX I

NUMBER OF TESTED CHIPS

A brief discussion of the number of tested chips is included here. The design was manufactured using 65 nm CMOS technology developed by TSMC with support from CMC Microsystems. We received 15 units packaged in a QP-QFN64-9mm-0.50mm 9 x 9 mm package from QPtechnologies (Tec). The wire-bonding diagram of the designed chip is shown in Fig. I-1. All of the units were tested and functioned as anticipated. Where possible, the measurement results presented in this work are the averages of the results gathered from 10 different measured units.

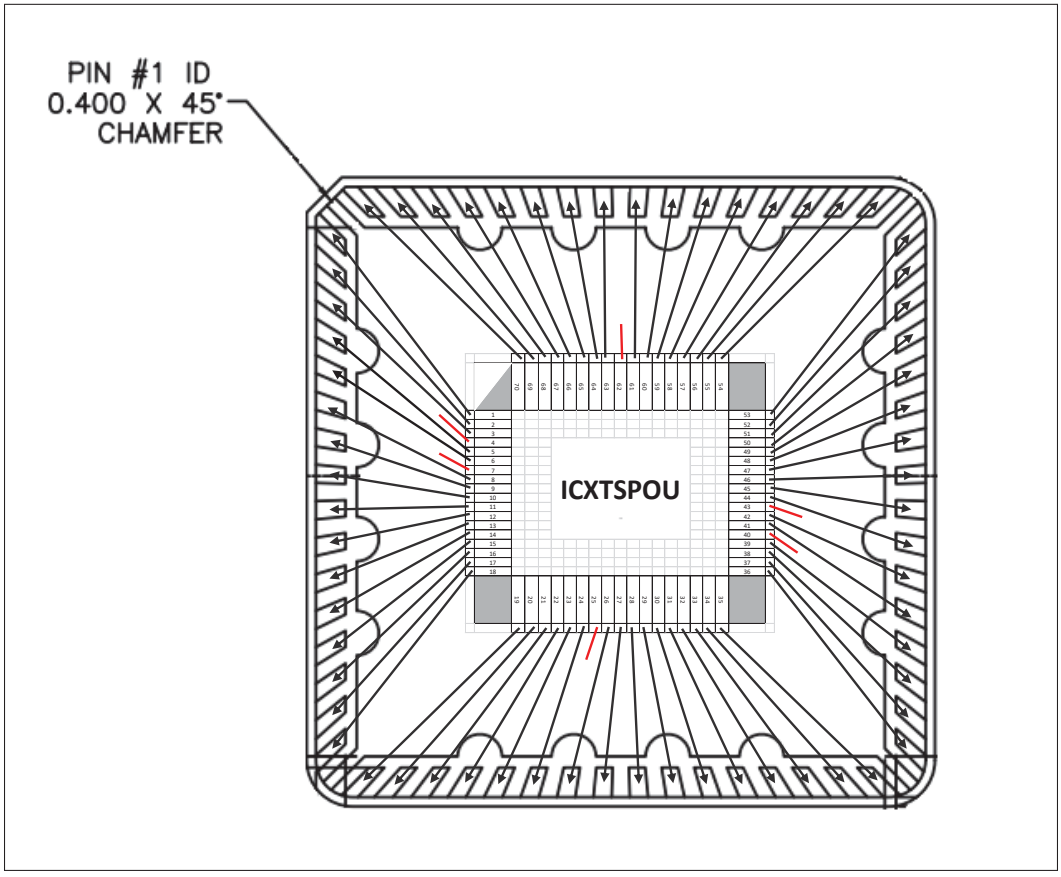

Figure-A I-1 Wire-bonding diagram of the designed chip.

BIBLIOGRAPHY

802.15.4z-2020 - IEEE Standard for Low-Rate Wireless Networks–Amendment 1: Enhanced Ultra Wideband (UWB) Physical Layers (PHYs) and Associated Ranging Techniques | IEEE Standard | IEEE Xplore. Retrieved https://ieeexplore.ieee.org/document/9179124.

DW1000 - Qorvo. Retrieved https://www.qorvo.com/products/p/DW1000.

SR 1000 Family | High-performance UWB Transceivers | Spark UWB Spark microsystems. Retrieved https://www.sparkmicro.com/products/#wireless-transceivers.

Technical Information - Technical Specs | QP Technologies. Retrieved https://www.qptechnologies.com/technical-resources/data-sheets/?doc=%2Fpdf%2FQFN_pdf%2FQP-QFN9X9-64-500%20PACKAGE.pdf.

Allidina, K. (2015). *A low power ultra wideband transceiver and sensor interface architecture for wireless sensor networks*. Retrieved https://search.proquest.com/openview/bd6be9b45dee2f495a578380fc5362b6/1?pq-origsite=gscholar&cbl=18750&diss=y.

Ammer, J. & Rabaey, J. (2006). The Energy-per-Useful-Bit metric for evaluating and optimizing sensor network physical layers. *2006 3rd Annual IEEE Communications Society on Sensor and Adhoc Communications and Networks, Secon 2006*, 2, 695–700. doi: 10.1109/SAHCN.2006.288533.

Arslan, H., Chen, Z. N. & Di Benedetto, M.-G. (2006). *Ultra wideband wireless communication*. John Wiley & Sons.

Barajas, E., Gómez, D., Mateo, D. & González, J. L. (2010). A 75 pJ/bit all-digital quadrature coherent IR-UWB transceiver in 0.18 μm CMOS. *2010 IEEE Radio Frequency Integrated Circuits Symposium*, pp. 197–200.

Chandrakasan, A. P., Lee, F. S., Wentzloff, D. D., Sze, V., Ginsburg, B. P., Mercier, P. P., Daly, D. C. & Blázquez, R. (2009). Low-power impulse UWB architectures and circuits. *Proceedings of the IEEE*, 97(2), 332–352. doi: 10.1109/JPROC.2008.2008787.

Commission, F. C. (2002). Revision of Part 15 of the Commission's Rules Regarding Ultra-Wideband Transmission Systems. *First Report and Order*, 02–48. Retrieved https://cir.nii.ac.jp/crid/1574231874694316800.

Crepaldi, M., Li, C., Fernandes, J. R. & Kinget, P. R. (2011). An ultra-wideband impulse-radio transceiver chipset using synchronized-OOK modulation. *IEEE Journal of Solid-State Circuits*, 46(10), 2284–2299.

Crepaldi, M., Angotzi, G. N. & Berdondini, L. (2019). A 0.34 mm2 1 Gb/s Non-Coherent UWB Receiver Architecture With Pulse Enhancement and Double PLL Clock/Data Packet Recovery. *IEEE Transactions on Circuits and Systems I: Regular Papers*, 66(7), 2735–2748. doi: 10.1109/TCSI.2019.2898042.

Daly, D. C., Mercier, P. P., Bhardwaj, M., Stone, A. L., Aldworth, Z. N., Daniel, T. L., Voldman, J., Hildebrand, J. G. & Chandrakasan, A. P. (2010). A pulsed UWB receiver SoC for insect motion control. *IEEE Journal of Solid-State Circuits*, 45(1), 153–166. doi: 10.1109/JSSC.2009.2034433.

Fontana, R. J. (2004). Recent system applications of short-pulse ultra-wideband (UWB) technology. *IEEE Transactions on Microwave Theory and Techniques*, 52(9 I), 2087–2104. doi: 10.1109/TMTT.2004.834186.

Geng, S., Liu, D., Li, Y., Zhuo, H., Rhee, W. & Wang, Z. (2015). A 13.3 mW 500 Mb/s IR-UWB transceiver with link margin enhancement technique for meter-range communications. *IEEE Journal of Solid-State Circuits*, 50(3), 669–678.

Group, I. . W. & others. (2003). Standard for Part 15.4: Wireless Medium Access Control Layer (MAC) and Physical Layer (PHY) Specifications for Low Rate Wireless Personal Area Networks (LR-WPANs). *IEEE Std*, 802(4).

Jha, A., Zhang, F., Hsieh, T. L., Gharpurey, R. & Kinget, P. R. (2010). A discrete-time digital-IF interference-robust ultrawideband pulse radio transceiver architecture. *IEEE Transactions on Circuits and Systems I: Regular Papers*, 57(2), 481–494. doi: 10.1109/TCSI.2009.2027802.

Kang, M. K. & Kim, T. W. (2012). CMOS IR-UWB receiver for pm 9.7-mm range finding in a multipath environment. *IEEE Transactions on Circuits and Systems II: Express Briefs*, 59(9), 538–542. doi: 10.1109/TCSII.2012.2206932.

Kim, N.-S. & Rabaey, J. M. (2016). A high data-rate energy-efficient triple-channel UWB-based cognitive radio. *IEEE Journal of Solid-State Circuits*, 51(4), 809–820.

Kong, S., Lee, S., Kim, C.-Y. & Hong, S. (2013). Wireless cooperative synchronization of coherent UWB MIMO radar. *IEEE transactions on microwave theory and techniques*, 62(1), 154–165.

Lee, G., Park, J., Jang, J., Jung, T. & Kim, T. W. (2019). An IR-UWB CMOS transceiver for high-data-rate, low-power, and short-range communication. *IEEE Journal of Solid-State Circuits*, 54(8), 2163–2174.

Liao, C.-F. & Liu, S.-I. (2007). A broadband noise-canceling CMOS LNA for 3.1–10.6-GHz UWB receivers. *IEEE Journal of Solid-State Circuits*, 42(2), 329–339.

Lin, Y. J., Song, H., Oh, S., Voroslakos, M., Kim, K., Chen, X., Wentzloff, D. D., Buzsaki, G., Park, S. Y. & Yoon, E. (2022). A 3.1-5.2GHz, Energy-Efficient Single Antenna, Cancellation-Free, Bitwise Time-Division Duplex Transceiver for High Channel Count Optogenetic Neural Interface. *IEEE Transactions on Biomedical Circuits and Systems*, 16(1), 52–63. doi: 10.1109/TBCAS.2021.3139891.

Liu, D., Ni, X., Zhou, R., Rhee, W. & Wang, Z. (2017). A 0.42-mW 1-Mb/s 3-to 4-GHz Transceiver in 0.18-mum CMOS With Flexible Efficiency, Bandwidth, and Distance Control for IoT Applications. *IEEE Journal of Solid-State Circuits*, 52(6), 1479–1494.

Liu, L., Sakurai, T. & Takamiya, M. (2011). A charge-domain auto-and cross-correlation based data synchronization scheme with power-and area-efficient PLL for impulse radio UWB receiver. *IEEE Journal of Solid-State Circuits*, 46(6), 1349–1359.

Miri, R., Zhou, L. & Heydari, P. (2008). Timing synchronization in impulse-radio UWB: Trends and challenges. *2008 Joint 6th International IEEE Northeast Workshop on Circuits and Systems and TAISA Conference*, pp. 221–224.

Park, P., Kim, S., Woo, S. & Kim, C. (2014). A centimeter resolution, 10 m range CMOS impulse radio radar for human motion monitoring. *IEEE Journal of Solid-State Circuits*, 49(5), 1125–1134.

Pelissier, M., Jantunen, J., Gomez, B., Arponen, J., Masson, G., Dia, S., Varteva, J. & Gary, M. (2011). A 112 Mb/s full duplex remotely-powered impulse-UWB RFID transceiver for wireless NV-memory applications. *IEEE Journal of Solid-State Circuits*, 46(4), 916–927.

Phan, A. T., Lee, J., Krizhanovskii, V., Le, Q., Han, S. K. & Lee, S. G. (2008). Energy-efficient low-complexity CMOS pulse generator for multiband UWB impulse radio. *IEEE Transactions on Circuits and Systems I: Regular Papers*, 55(11), 3552–3563. doi: 10.1109/TCSI.2008.925821.

Piraghaj, S. F. & Saeedi, S. (2019). Analysis of Timing Accuracy and Sensitivity in a RF Correlation-Based Impulse Radio Receiver With Phase Interpolation for Data Synchronization. *IEEE Transactions on Circuits and Systems I: Regular Papers*, 66(7), 2749–2762.

Ryckaert, J., Verhelst, M., Badaroglu, M., D'Amico, S., De Heyn, V., Desset, C., Nuzzo, P., Van Poucke, B., Wambacq, P., Baschirotto, A. & others. (2007). A CMOS ultra-wideband receiver for low data-rate communication. *IEEE Journal of Solid-State Circuits*, 42(11), 2515–2527.

Shams, N., Kakhki, A. P. & Nabki, F. (2019). Reconfigurable IR-UWB current mode switched receiver for IoT applications. *2019 26th IEEE International Conference on Electronics, Circuits and Systems, ICECS 2019*, 9–12. doi: 10.1109/ICECS46596.2019.8965095.

Solda, S., Caruso, M., Bevilacqua, A., Gerosa, A., Vogrig, D. & Neviani, A. (2011). A 5 Mb/s UWB-IR Transceiver Front-End for Wireless Sensor Networks in 0.13mum CMOS. *IEEE Journal of Solid-State Circuits*, 46(7), 1636–1647.

Song, H., Liu, D., Zhang, Y., Rhee, W. & Wang, Z. (2019). A 6.5–8.1-GHz Communication/Ranging VWB Transceiver for Secure Wireless Connectivity With Enhanced Bandwidth Efficiency and $\Delta\Sigma$ Energy Detection. *IEEE Journal of Solid-State Circuits*, 55(2), 219–232.

Terada, T., Yoshizumi, S., Muqsith, M., Sanada, Y. & Kuroda, T. (2006). A CMOS ultra-wideband impulse radio transceiver for 1-mb/s data communications and/spl plusmn/2.5-cm range finding. *IEEE Journal of Solid-State Circuits*, 41(4), 891–898.

Thoppay, P. E., Dehollain, C., Green, M. M. & Declercq, M. J. (2011). A 0.24-nJ/bit super-regenerative pulsed UWB receiver in 0.18-μm CMOS. *IEEE Journal of Solid-State Circuits*, 46(11), 2623–2634. doi: 10.1109/JSSC.2011.2166434.

Van Helleputte, N., Verhelst, M., Dehaene, W. & Gielen, G. (2009). A reconfigurable, 130 nm CMOS 108 pJ/pulse, fully integrated IR-UWB receiver for communication and precise ranging. *IEEE Journal of Solid-State Circuits*, 45(1), 69–83.

Vauche, R., Muhr, E., Fourquin, O., Bourdel, S., Gaubert, J., Dehaese, N., Meillere, S., Barthelemy, H. & Ouvry, L. (2017). A 100 MHz PRF IR-UWB CMOS Transceiver with Pulse Shaping Capabilities and Peak Voltage Detector. *IEEE Transactions on Circuits and Systems I: Regular Papers*, 64(6), 1612–1625. doi: 10.1109/TCSI.2017.2669902.

Vigraham, B. & Kinget, P. R. (2014). A self-duty-cycled and synchronized UWB pulse-radio receiver SoC with automatic threshold-recovery based demodulation. *IEEE Journal of Solid-State Circuits*, 49(3), 581–594.

Wang, X., Yu, Y., Busze, B., Pflug, H., Young, A., Huang, X., Zhou, C., Konijnenburg, M., Philips, K. & De Groot, H. (2012). A meter-range UWB transceiver chipset for around-the-head audio streaming. *2012 IEEE International Solid-State Circuits Conference*, pp. 450–452.

Xiong, F. (2006). *Digital Modulation Techniques, (Artech House Telecommunications Library)*. Artech House, Inc.

Zhang, F., Jha, A., Gharpurey, R. & Kinget, P. (2009). An agile, ultra-wideband pulse radio transceiver with discrete-time wideband-IF. *IEEE journal of solid-state circuits*, 44(5), 1336–1351.

Zheng, Y., Arasu, M. A., Wong, K. W., The, Y. J., Suan, A. P. H., Tran, D. D., Yeoh, W. G. & Kwong, D. L. (2008). A 0.18μm CMOS 802.15.4a UWB transceiver for communication and localization. *Digest of Technical Papers - IEEE International Solid-State Circuits Conference*, 51, 117–119. doi: 10.1109/ISSCC.2008.4523085.

Zhou, L., Chen, Z., Wang, C.-C., Tzeng, F., Jain, V. & Heydari, P. (2011). A 2-Gb/s 130-nm CMOS RF-correlation-based IR-UWB transceiver front-end. *IEEE Transactions on Microwave Theory and Techniques*, 59(4), 1117–1130.

Zhuo, W., Li, X., Shekhar, S., Embabi, S. H. K., de Gyvez, J. P., Allstot, D. J. & Sanchez-Sinencio, E. (2005). A capacitor cross-coupled common-gate low-noise amplifier. *IEEE Transactions on Circuits and Systems II: Express Briefs*, 52(12), 875–879.